

# JGR Atmospheres

## RESEARCH ARTICLE

10.1029/2024JD041168

## Ozone Formation Sensitivity to Precursors and Lightning in the Tropical Troposphere Based on Airborne Observations



### Key Points:

- $\alpha(\text{CH}_3\text{O}_2)$  correlated with NO is a powerful metric for indicating  $\text{O}_3$  sensitivity and is valid throughout the troposphere
- $\text{O}_3$  chemistry in the remote tropical lower troposphere is found to be  $\text{NO}_x$ -sensitive
- NO emissions from lightning drive  $\text{O}_3$  sensitivity in the tropical upper troposphere and induce highly VOC-sensitive chemistry

### Supporting Information:

Supporting Information may be found in the online version of this article.

### Correspondence to:

C. M. Nussbaumer,  
[clara.nussbaumer@mpic.de](mailto:clara.nussbaumer@mpic.de)

### Citation:

Nussbaumer, C. M., Kohl, M., Pozzer, A., Tadic, I., Rohloff, R., Marno, D., et al. (2024). Ozone formation sensitivity to precursors and lightning in the tropical troposphere based on airborne observations. *Journal of Geophysical Research: Atmospheres*, 129, e2024JD041168. <https://doi.org/10.1029/2024JD041168>

Received 12 MAR 2024

Accepted 8 JUL 2024

### Author Contributions:

**Conceptualization:** Clara



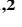



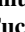





M. Nussbaumer, Horst Fischer

**Data curation:** Clara M. Nussbaumer, Matthias Kohl, Andrea Pozzer, Ivan Tadic, Roland Rohloff, Daniel Marno, Hartwig Harder, Helmut Ziereis, Andreas Zahn, Florian Obersteiner, Andreas Hofzumahaus, Hendrik Fuchs, Christopher Künstler, William H. Brune, Tom B. Ryerson, Jeff Peischl, Chelsea R. Thompson, Ilann Bourgeois

**Formal analysis:** Clara M. Nussbaumer

**Funding acquisition:** Jos Lelieveld

**Investigation:** Clara M. Nussbaumer

Clara M. Nussbaumer<sup>1</sup> , Matthias Kohl<sup>1</sup> , Andrea Pozzer<sup>1,2</sup> , Ivan Tadic<sup>1</sup>, Roland Rohloff<sup>1</sup>, Daniel Marno<sup>1</sup>, Hartwig Harder<sup>1</sup>, Helmut Ziereis<sup>3</sup> , Andreas Zahn<sup>4</sup> , Florian Obersteiner<sup>4</sup> , Andreas Hofzumahaus<sup>5</sup> , Hendrik Fuchs<sup>5</sup>, Christopher Künstler<sup>5</sup>, William H. Brune<sup>6</sup> , Tom B. Ryerson<sup>7</sup> , Jeff Peischl<sup>8,9</sup> , Chelsea R. Thompson<sup>8</sup> , Ilann Bourgeois<sup>8,9,10</sup>, Jos Lelieveld<sup>1,2</sup> , and Horst Fischer<sup>1</sup>

<sup>1</sup>Department of Atmospheric Chemistry, Max Planck Institute for Chemistry, Mainz, Germany, <sup>2</sup>Climate and Atmosphere Research Center, The Cyprus Institute, Nicosia, Cyprus, <sup>3</sup>Deutsches Zentrum für Luft- und Raumfahrt (DLR), Institut für Physik der Atmosphäre, Oberpfaffenhofen, Germany, <sup>4</sup>Institute of Meteorology and Climate Research (IMK), Karlsruhe Institute of Technology, Karlsruhe, Germany, <sup>5</sup>Institute of Energy and Climate Research – Troposphere (IEK-8), Forschungszentrum Jülich GmbH, Jülich, Germany, <sup>6</sup>Department of Meteorology and Atmospheric Science, Pennsylvania State University, University Park, PA, USA, <sup>7</sup>Scientific Aviation, Boulder, CO, USA, <sup>8</sup>National Oceanic and Atmospheric Administration (NOAA) Chemical Sciences Laboratory (CSL), Boulder, CO, USA, <sup>9</sup>Cooperative Institute for Research in Environmental Sciences, University of Colorado Boulder, Boulder, CO, USA, <sup>10</sup>Now at Université Savoie Mont Blanc, INRAE, CARTELE, Thonon-les-Bains, France

**Abstract** Tropospheric ozone ( $\text{O}_3$ ) is an important greenhouse gas that is also hazardous to human health. The formation of  $\text{O}_3$  is sensitive to the levels of its precursors  $\text{NO}_x$  ( $\equiv \text{NO} + \text{NO}_2$ ) and peroxy radicals, for example, generated by the oxidation of volatile organic compounds (VOCs). A better understanding of this sensitivity will show how changes in the levels of these trace gases could affect  $\text{O}_3$  levels today and in the future, and thus air quality and climate. In this study, we investigate  $\text{O}_3$  sensitivity in the tropical troposphere based on in situ observations of NO,  $\text{HO}_2$  and  $\text{O}_3$  from four research aircraft campaigns between 2015 and 2023. These are OMO (Oxidation Mechanism Observations), ATom (Atmospheric Tomography Mission), CAFE Africa (Chemistry of the Atmosphere Field Experiment in Africa) and CAFE Brazil, in combination with simulations using the EMAC atmospheric chemistry—climate model. We use the metric  $\alpha(\text{CH}_3\text{O}_2)$  together with NO to investigate the  $\text{O}_3$  formation sensitivity. We show that  $\text{O}_3$  formation is generally  $\text{NO}_x$ -sensitive in the lower and middle tropical troposphere and is in a transition regime in the upper troposphere. By distinguishing observations impacted by lightning or not we show that NO from lightning is the most important driver of  $\text{O}_3$  sensitivity in the tropics.  $\text{NO}_x$ -sensitive chemistry predominates in regions without lightning impact, with  $\alpha(\text{CH}_3\text{O}_2)$  ranging between 0.56 and 0.82 and observed average  $\text{O}_3$  levels between 35 and 55 ppbv. Areas affected by lightning exhibit strongly VOC-sensitive  $\text{O}_3$  chemistry with  $\alpha(\text{CH}_3\text{O}_2)$  of about 1 and average  $\text{O}_3$  levels between 55 and 80 ppbv.

**Plain Language Summary** Ozone ( $\text{O}_3$ ) in the troposphere is both an air pollutant and a greenhouse gas. It is formed from nitrogen oxides ( $\text{NO}_x$ ) and volatile organic compounds (VOCs). The formation can be sensitive to either of these precursors depending on their abundance. Considering the high relevance of  $\text{O}_3$  in regard to human health and global warming, it is important to understand this sensitivity of  $\text{O}_3$  formation, which allows to predict future changes in  $\text{O}_3$ . Here, we investigate  $\text{O}_3$  formation sensitivity toward  $\text{NO}_x$  and VOCs in the tropical troposphere based on aircraft measurements during four research campaigns between 2015 and 2023, and a global model. We include observations of NO,  $\text{HO}_2$  (hydroperoxyl radicals) and  $\text{O}_3$  over South America, the Middle East and the Pacific, Atlantic and Indian Ocean. We find that  $\text{O}_3$  formation is sensitive to  $\text{NO}_x$  in the lower tropical troposphere. In the upper tropical troposphere, lightning events control  $\text{O}_3$  chemistry and promote strong VOC-sensitive  $\text{O}_3$  formation.

© 2024. The Author(s).

This is an open access article under the terms of the [Creative Commons Attribution-NonCommercial-NoDerivs License](https://creativecommons.org/licenses/by/4.0/), which permits use and distribution in any medium, provided the original work is properly cited, the use is non-commercial and no modifications or adaptations are made.

## 1. Introduction

Ozone ( $\text{O}_3$ ) in the stratosphere is essential to life on this planet through its shielding of the Earth's surface from the sun's shortwave radiation (Staelin et al., 2001). In contrast, in the troposphere  $\text{O}_3$  has adverse effects for plants, human health and the climate (Ainsworth et al., 2012; Nuvolone et al., 2018).  $\text{O}_3$  is an important anthropogenic greenhouse gas (after  $\text{CO}_2$  and  $\text{CH}_4$ ). Its impact on global warming is strongest in the upper troposphere. At these

**Project administration:** Jos Lelieveld, Horst Fischer  
**Supervision:** Horst Fischer  
**Visualization:** Clara M. Nussbaumer  
**Writing – original draft:** Clara M. Nussbaumer  
**Writing – review & editing:** Clara M. Nussbaumer, Matthias Kohl, Andrea Pozzer, Ivan Tadic, Hartwig Harder, Helmut Ziereis, Andreas Zahn, Florian Obersteiner, Andreas Hofzumahaus, Hendrik Fuchs, Jeff Peischl, Jos Lelieveld, Horst Fischer

altitudes, O<sub>3</sub> is most abundant (relative to tropospheric levels), temperatures are coldest and concentrations of water vapor, the predominant natural greenhouse gas, are low (Cooper et al., 2014; Iglesias-Suarez et al., 2018; IPCC, 2023). This influence of O<sub>3</sub> on the radiative budget is particularly pronounced in tropical latitudes (30°S to 30°N), which are characterized by large O<sub>3</sub> precursor emissions due to strong lightning and particularly low temperatures due to the high altitude of the tropical tropopause (Iglesias-Suarez et al., 2018; Laciš et al., 1990; Skeie et al., 2020). O<sub>3</sub> is additionally an important precursor for OH radicals, which in turn control the atmospheric oxidizing capacity (Lelieveld et al., 2016).

Primary sources of ozone in the troposphere include transport from the stratosphere and photochemical formation. While the exact source distribution has not yet been fully understood up to this point, it is almost certain that photochemical production is the dominant source of O<sub>3</sub> in the troposphere (Archibald et al., 2020; Cooper et al., 2014; Lelieveld & Dentener, 2000). Nitrogen oxides (NO<sub>x</sub> ≡ NO + NO<sub>2</sub>) and volatile organic compounds (VOCs) are photochemical precursors for O<sub>3</sub> in the troposphere. NO<sub>x</sub> is mostly emitted in the form of NO and converted to NO<sub>2</sub> in the presence of peroxy radicals (mostly HO<sub>2</sub> and CH<sub>3</sub>O<sub>2</sub>), shown in Reactions R1 and R2. Peroxy radicals in turn are formed through oxidation of VOCs or carbon monoxide (CO) by OH radicals (Crutzen, 1988; Nussbaumer & Cohen, 2020; Pusede et al., 2015).



NO<sub>2</sub> forms O<sub>3</sub> in the presence of sunlight and oxygen from the air via Reaction R3.



Precursor sources at the surface are combustion processes (vehicle engines, vessels, industrial activities, etc.), biomass burning and soil emissions for NO and mostly evaporative emissions, including volatile chemical products (personal care products, detergents, etc.), as well as biogenic emissions from vegetated areas for VOCs (McDonald et al., 2018; Pusede et al., 2015). Aircraft and lightning are sources of NO at higher altitudes in the troposphere.

Depending on the precursor concentrations, O<sub>3</sub> formation can be sensitive to either NO<sub>x</sub> or VOCs, the latter represented by peroxy radicals. A detailed analysis and discussion of our current understanding of O<sub>3</sub> sensitivity can be found in Nussbaumer et al. (2023). Briefly, for low NO<sub>x</sub>, referred to as NO<sub>x</sub>-sensitive O<sub>3</sub> chemistry, VOCs and therefore peroxy radicals are present in excess. Peroxy radicals undergo Reactions R1 and R2 with NO and further react with themselves in radical recombination reactions or undergo auto oxidation. O<sub>3</sub> formation generally increases with increasing NO. O<sub>3</sub> chemistry is VOC-sensitive when NO<sub>x</sub> is available in excess. A maximum level of ozone production is reached when the available peroxy radicals react with NO to form NO<sub>2</sub>. The impact of increases in NO<sub>x</sub> on O<sub>3</sub> concentrations for VOC-sensitive O<sub>3</sub> chemistry changes with the altitude, which we hypothesize is due to the fraction of NO<sub>2</sub>. At the surface, O<sub>3</sub> formation decreases with increasing NO<sub>x</sub> due to the reaction of OH radicals with NO<sub>2</sub> (instead of VOCs to generate peroxy radicals), which becomes relevant when NO<sub>x</sub> is more abundant than reactive VOCs. Observations of decreasing O<sub>3</sub> at high NO<sub>x</sub> are often reported in literature, for example, Nussbaumer and Cohen (2020), Sicard et al. (2020) or Gough and Anderson (2022). In the upper troposphere, the reaction of NO<sub>2</sub> with OH only plays a minor role—likely because daytime NO<sub>2</sub> is low as the NO<sub>x</sub> equilibrium is shifted toward NO. Consequently, O<sub>3</sub> is much less responsive to NO changes. We have shown this effect of O<sub>3</sub> in the upper troposphere in Nussbaumer et al. (2023).

In order to understand and predict the response of O<sub>3</sub> toward changes in NO<sub>x</sub> and VOCs, it is essential to investigate which precursor O<sub>3</sub> is sensitive to, given its importance for air quality and climate. Various metrics exist to determine which sensitivity prevails, including the response of ozone production P(O<sub>3</sub>) to changes in NO<sub>x</sub>, the weekend effect, the HCHO to NO<sub>2</sub> ratio, the HNO<sub>3</sub> to H<sub>2</sub>O<sub>2</sub> ratio and the LNO<sub>x</sub> to LRO<sub>x</sub> ratio. As described in the previous paragraph, P(O<sub>3</sub>) increases with NO<sub>x</sub> for NO<sub>x</sub>-sensitive and decreases with NO<sub>x</sub> for VOC-sensitive O<sub>3</sub> chemistry. The driver for the latter decrease is the increasing importance of the (HO<sub>x</sub> cycle) terminating reaction NO<sub>2</sub> + OH with increasing NO<sub>x</sub>. This context is used when investigating the weekend effect (e.g., Fujita et al. (2003); Gough and Anderson (2022)). A smaller number of transporter trucks and commuter

traffic during weekends leads to lower  $\text{NO}_x$  concentrations. When  $\text{O}_3$  reductions are observed along these  $\text{NO}_x$  conditions,  $\text{O}_3$  formation is  $\text{NO}_x$ -sensitive. In contrast,  $\text{O}_3$  enhancements on weekends indicate VOC-sensitive chemistry. The metric  $\text{HCHO}/\text{NO}_2$  represents the ratio of VOCs and  $\text{NO}_x$  (e.g., Sillman (1995); Tonnesen and Dennis (2000)). High values indicate the prevalence of VOCs and, therefore,  $\text{NO}_x$ -sensitive  $\text{O}_3$  chemistry. Low values highlight the increased availability of  $\text{NO}_x$  and VOC-sensitive  $\text{O}_3$  formation. The  $\text{HCHO}/\text{NO}_2$  ratio requires knowledge about experimental thresholds for each sensitivity region. For example, Duncan et al. (2010) suggest  $\text{HCHO}/\text{NO}_2 < 1$  for VOC-sensitive and  $\text{HCHO}/\text{NO}_2 > 2$  for  $\text{NO}_x$ -sensitive  $\text{O}_3$  formation. The  $\text{HNO}_3/\text{H}_2\text{O}_2$  ratio compares the two major termination pathways of the  $\text{HO}_x$  cycle (e.g., Sillman (1995); Sillman and He (2002); Vermeuel et al. (2019)). These are the loss of  $\text{NO}_2$  via the reaction with OH (forming  $\text{HNO}_3$ ) and the loss of  $\text{HO}_2$  via self-reaction (forming  $\text{H}_2\text{O}_2$ ). The prevalence of  $\text{NO}_x$  promotes the termination via  $\text{NO}_2$  loss, representing VOC-sensitive  $\text{O}_3$  chemistry. The termination via  $\text{HO}_2$  recombination becomes dominant for prevailing VOCs over  $\text{NO}_x$ , indicating  $\text{NO}_x$ -sensitive  $\text{O}_3$  chemistry. An extension of  $\text{HNO}_3/\text{H}_2\text{O}_2$  is given by the  $\text{LNO}_x/\text{LRO}_x$  ratio, which compares the loss of  $\text{NO}_x$  ( $\text{LNO}_x$ ) with the loss of  $\text{RO}_x$  ( $\text{LRO}_x$ ) (e.g., Schroeder et al., 2017; Sourì et al., 2020, 2023). The loss of  $\text{NO}_x$  is hereby given by the reaction of  $\text{NO}_2$  with OH and is equal to considering the formation of  $\text{HNO}_3$ . In addition to the formation of  $\text{H}_2\text{O}_2$  via  $\text{HO}_2$ , the loss of  $\text{RO}_x$  includes the self-reaction of  $\text{RO}_2$  and the cross-combination of  $\text{HO}_2$  and  $\text{RO}_2$ . Similar to the ratios  $\text{HCHO}/\text{NO}_2$  and  $\text{HNO}_3/\text{H}_2\text{O}_2$ , an experimental threshold is needed to identify the transition point, for example,  $\text{LNO}_x/\text{LRO}_x \sim 2.7$  as given by Sourì et al. (2020). Studies by Schroeder et al. (2017) and Sourì et al. (2023) indicate that difficulties in the use of  $\text{HCHO}/\text{NO}_2$  can be addressed by the application of  $\text{LNO}_x/\text{LRO}_x$ , which they found to be superior for the identification of near surface ozone formation sensitivity. A detailed review and comparison of the most common metrics in the literature is presented in Liu and Shi (2021) for the surface and Nussbaumer et al. (2023) for the global troposphere. We found that most of these metrics are only applicable at the surface, and particularly not in the upper troposphere. Mixing ratios of trace gases vary significantly throughout the troposphere and definitions for the surface, for example,  $\text{P}(\text{O}_3)$  changes with  $\text{NO}_x$  or experimental thresholds for the  $\text{HCHO}/\text{NO}_2$ ,  $\text{HNO}_3/\text{H}_2\text{O}_2$  or  $\text{LNO}_x/\text{LRO}_x$  ratios might not apply at high altitudes.  $\text{P}(\text{O}_3)$ ,  $\text{HNO}_3/\text{H}_2\text{O}_2$  and  $\text{LNO}_x/\text{LRO}_x$  consider the dominance of the terminating reaction  $\text{NO}_2 + \text{OH}$  (forming  $\text{HNO}_3$ ) as an indicator for VOC-sensitive  $\text{O}_3$  chemistry. At high altitudes,  $\text{NO}_2$  concentrations tend to be low and so does the  $\text{NO}_x$  loss via the pressure-dependent reaction  $\text{NO}_2 + \text{OH} (+\text{M})$ . As a consequence, we hypothesize that  $\text{P}(\text{O}_3)$  as a function of NO increases beyond the transition point between  $\text{NO}_x$ - and VOC-sensitive  $\text{O}_3$  formation sensitivity in the upper troposphere. We have shown this in Figure S10 of Nussbaumer et al. (2023), which presents  $\text{P}(\text{O}_3)$  and  $\text{L}(\text{NO}_x)$  versus NO for upper tropical tropospheric data simulated by the general circulation model EMAC. The loss of  $\text{NO}_x$  via  $\text{NO}_2 + \text{OH}$  is less than 5% of  $\text{P}(\text{O}_3)$  over the entire range of NO from 0 to 1 ppbv. Therefore,  $\text{L}(\text{NO}_x)$  does not impact the course of  $\text{P}(\text{O}_3)$  as a function of NO and it can therefore not indicate the transition from  $\text{NO}_x$ - to VOC-sensitivity. The same applies to  $\text{HNO}_3/\text{H}_2\text{O}_2$  and  $\text{LNO}_x/\text{LRO}_x$ . Further drawbacks of these metrics at high altitudes are that knowledge of  $\text{NO}_2$  mixing ratios is required, which does not allow for the application of in situ measurements. It was shown that  $\text{NO}_2$  measurements in the upper troposphere suffer from thermal artifacts from peroxy nitrates, independent of the measurement principle (Shah et al., 2023). Instead, we have developed a new metric,  $\alpha(\text{CH}_3\text{O}_2)$ , to determine  $\text{O}_3$  sensitivity, which is valid throughout the entire troposphere (Nussbaumer et al., 2021a, 2022).  $\alpha(\text{CH}_3\text{O}_2)$  presents the ratio of methyl peroxy radicals  $\text{CH}_3\text{O}_2$  (a proxy for VOCs) which react with NO and promote  $\text{O}_3$  formation in competition with the peroxy radical self-reaction which inhibits  $\text{O}_3$  formation.  $\text{O}_3$  formation is  $\text{NO}_x$ -sensitive when  $\alpha(\text{CH}_3\text{O}_2)$  increases with increasing NO. In this case, peroxy radicals are present in excess, and  $\text{O}_3$  production is sensitive only to changes in NO ( $\text{NO}_x$ -sensitive).  $\text{O}_3$  chemistry is VOC-sensitive when  $\alpha(\text{CH}_3\text{O}_2)$  and, at the same time  $\text{O}_3$  formation, become unresponsive to changes in NO. Instead,  $\text{O}_3$  production is sensitive only to changes in VOCs (VOC-sensitive) and, consequently, peroxy radicals. We present more details including the calculation of  $\alpha(\text{CH}_3\text{O}_2)$  in Section 2.1.  $\alpha(\text{CH}_3\text{O}_2)$  indicates the transition from  $\text{NO}_x$ - to VOC-sensitive  $\text{O}_3$  formation sensitivity at around 0.1 ppbv NO for Figure S10 in Nussbaumer et al. (2023).

$\alpha(\text{CH}_3\text{O}_2)$  was originally proposed as an indicator for formaldehyde formation and applied to three stationary ground-site measurements across Europe in Cyprus, Germany and Finland (Nussbaumer, Crowley, et al., 2021).  $\alpha(\text{CH}_3\text{O}_2)$  identified  $\text{NO}_x$ -sensitive  $\text{O}_3$  chemistry in southeastern Europe and VOC-sensitive  $\text{O}_3$  chemistry in central Europe, which is in line with results obtained via the  $\text{HCHO}$  to  $\text{NO}_2$  ratio, a metric dating back to studies by Sillman (1995). In Nussbaumer et al. (2022), we used  $\alpha(\text{CH}_3\text{O}_2)$  to indicate a change in upper tropospheric  $\text{O}_3$  sensitivity in response to reduced air traffic (and a 55% reduction in  $\text{NO}_x$  mixing ratios) during the COVID-19 lockdowns over Europe, which common metrics would have failed to identify. We have recently investigated

O<sub>3</sub> sensitivity in the upper tropical troposphere based on modeling simulations by a general circulation model and found lightning as the most important driver of VOC-sensitive O<sub>3</sub> chemistry (Nussbaumer et al., 2023). Generally, these studies have underlined that NO<sub>x</sub> is most relevant in O<sub>3</sub> formation and sensitivity and that the abundance of VOCs only plays a subordinate role.

There are numerous studies that have investigated O<sub>3</sub> sensitivity to NO<sub>x</sub> and VOC levels at the surface and they almost exclusively focus on urban areas (Akimoto & Tanimoto, 2022; Jaffe et al., 2022; Li et al., 2019; Zhao et al., 2022). While this is highly relevant with respect to air quality and human health, it is also important to investigate more remote locations particularly in regard to future emission changes. For example, with increasing temperatures and decreasing precipitation one could expect to see increases in biomass burning, resulting in emission of NO<sub>x</sub> in the remote rainforest (Bray et al., 2021). In combination with the high levels of VOCs in these areas, O<sub>3</sub> could increase drastically locally, and in turn harm the natural vegetation and agricultural crops (Ainsworth et al., 2012; Pope et al., 2020). At the same time, ongoing industrialization in the Global South will likely impact ozone concentrations in the tropical troposphere (Gaudel et al., 2024). In contrast to surface-based analyzes, research on O<sub>3</sub> sensitivity in the upper troposphere is scant and has not been investigated in detail since the studies of Brasseur et al. (1996), Jaeglé et al. (1998), Wennberg et al. (1998), and Jaeglé et al. (1999) around 25 years ago, who concluded that O<sub>3</sub> chemistry was NO<sub>x</sub>-sensitive in the upper troposphere over the United States based on box-model simulations. Of note, the observations for high NO<sub>x</sub> did not match the model predictions in Jaeglé et al. (1998, 1999). We suggest that O<sub>3</sub> production is an unsuitable metric for indicating O<sub>3</sub> sensitivity at high altitudes. This could be (partly) due to the terminating reaction OH + NO<sub>2</sub> (forming HNO<sub>3</sub>), which does not seem to play a significant role for low NO<sub>2</sub> mixing ratios in the upper troposphere. Findings by Jaeglé et al. (1998, 1999) and Nussbaumer et al. (2023) suggest that P(O<sub>3</sub>) is an unsuitable indicator for determining O<sub>3</sub> formation sensitivity at high tropospheric altitudes.

This study investigates O<sub>3</sub> chemistry in the tropical troposphere based on airborne observations during four aircraft campaigns, namely OMO, ATom, CAFE Africa and CAFE Brazil, between 2015 and 2023. We compare in situ observations with modeled data by the ECHAM5/MESy2 Atmospheric Chemistry (EMAC) model and we investigate the differences in trace gas concentrations and vertical profiles between the individual campaigns (and regions). We use  $\alpha(\text{CH}_3\text{O}_2)$  to identify O<sub>3</sub> sensitivity towards its precursors in the tropical troposphere, with a particular focus on the role of lightning.

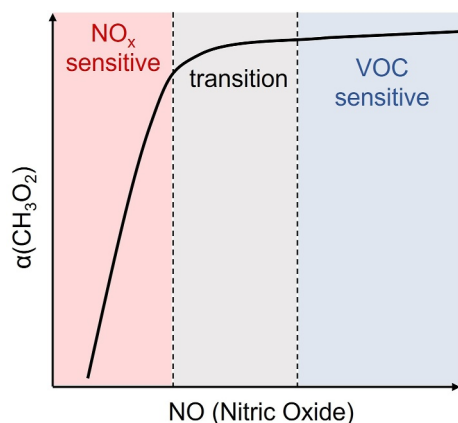
While we have previously analyzed O<sub>3</sub> chemistry in the upper tropical troposphere based on model simulations (Nussbaumer et al., 2023), this is the first study to investigate the question of O<sub>3</sub> sensitivity at these altitudes based on in situ observations using the metric  $\alpha(\text{CH}_3\text{O}_2)$ . To our knowledge,  $\alpha(\text{CH}_3\text{O}_2)$  is currently the only available metric reliably indicating which precursor O<sub>3</sub> is sensitive to at altitudes at which common tools fail and the impact of O<sub>3</sub> as a greenhouse gas is strongest.

## 2. Observation and Methods

### 2.1. O<sub>3</sub> Sensitivity Metric $\alpha(\text{CH}_3\text{O}_2)$

$\alpha(\text{CH}_3\text{O}_2)$  was originally developed for identifying HCHO (formaldehyde) production pathways. It presents the share of CH<sub>3</sub>O<sub>2</sub> (methyl peroxy radicals) reacting with NO or OH radicals forming HCHO versus the peroxy self-reaction (CH<sub>3</sub>O<sub>2</sub> + HO<sub>2</sub>) forming CH<sub>3</sub>OOH (Nussbaumer, Crowley, et al., 2021). The reaction of CH<sub>3</sub>O<sub>2</sub> with NO also yields NO<sub>2</sub>, which forms O<sub>3</sub> via Reaction R3. The pathway of CH<sub>3</sub>O<sub>2</sub> with NO forming methyl nitrate is negligibly small and does not impact O<sub>3</sub> formation. The reaction of CH<sub>3</sub>O<sub>2</sub> with HO<sub>2</sub> represents a termination reaction of the O<sub>3</sub> formation process (which is relevant for a low-NO<sub>x</sub> environment). The reaction of CH<sub>3</sub>O<sub>2</sub> with OH contributes to HCHO, but not to O<sub>3</sub> formation, and generally only plays a minor role compared to the pathway via NO and HO<sub>2</sub>. Therefore, it can be disregarded when studying O<sub>3</sub> sensitivity. Hence,  $\alpha(\text{CH}_3\text{O}_2)$  is calculated via Equation R4. We only use positive values for determining  $\alpha(\text{CH}_3\text{O}_2)$  to ensure that the resulting value is between 0 and 1. The rate constants  $k$  were obtained from the IUPAC database with  $k(\text{CH}_3\text{O}_2 + \text{HO}_2) = 3.8 \times 10^{-13} \exp(780/T)$  and  $k(\text{CH}_3\text{O}_2 + \text{NO}) = 2.3 \times 10^{-12} \exp(360/T)$ .  $T$  represents the ambient temperature in Kelvin (IUPAC, 2024).

$$\alpha(\text{CH}_3\text{O}_2) = \frac{k_{\text{CH}_3\text{O}_2+\text{NO}} \times [\text{NO}]}{k_{\text{CH}_3\text{O}_2+\text{NO}} \times [\text{NO}] + k_{\text{CH}_3\text{O}_2+\text{HO}_2} \times [\text{HO}_2]} \quad (\text{R4})$$



**Figure 1.** Identifying the dominant O<sub>3</sub> sensitivity using  $\alpha(\text{CH}_3\text{O}_2)$  (adapted from Nussbaumer, 2023). This is a simplified overview for explanation purposes. The absolute numbers for  $\alpha(\text{CH}_3\text{O}_2)$  and NO vary depending on the studied region.

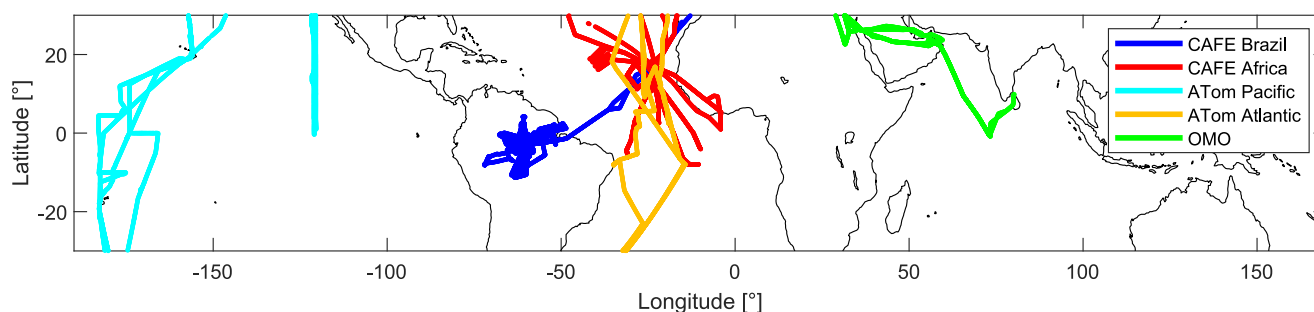
A detailed description of  $\alpha(\text{CH}_3\text{O}_2)$  can be found in Nussbaumer, Crowley, et al. (2021), Nussbaumer et al. (2022), and Nussbaumer et al. (2023). Briefly, for low NO<sub>x</sub> concentrations, CH<sub>3</sub>O<sub>2</sub> react with both NO and HO<sub>2</sub> and increases in NO lead to increases in  $\alpha(\text{CH}_3\text{O}_2)$ . O<sub>3</sub> chemistry is NO<sub>x</sub>-sensitive. For high NO<sub>x</sub> concentrations, most available CH<sub>3</sub>O<sub>2</sub> reacts with NO and changes in NO have no impact on  $\alpha(\text{CH}_3\text{O}_2)$ , as O<sub>3</sub> sensitivity is limited by the availability of peroxy radicals (which represent the abundance of VOCs). Figure 1 schematically shows how to use  $\alpha(\text{CH}_3\text{O}_2)$  to identify prevailing O<sub>3</sub> sensitivity (Nussbaumer, 2023). O<sub>3</sub> concentrations increase with increasing NO<sub>x</sub> when O<sub>3</sub> chemistry is NO<sub>x</sub>-sensitive. For VOC-sensitive O<sub>3</sub> chemistry at the surface, O<sub>3</sub> formation decreases with increasing NO<sub>x</sub> due to the reaction of OH and NO<sub>2</sub>. In the upper troposphere, O<sub>3</sub> concentrations reach a maximum and remain unresponsive to changes in NO<sub>x</sub>.  $\alpha(\text{CH}_3\text{O}_2)$  is currently the only available metric that identifies O<sub>3</sub> formation sensitivity based on in situ observations throughout the troposphere. While HO<sub>2</sub> measurements remain to be a challenge, uncertainties will only impact the exact definition of the transition point between NO<sub>x</sub>- and VOC-sensitive O<sub>3</sub> formation, which does not affect the overall result.

## 2.2. Aircraft Campaigns

Figure 2 presents an overview of the flight tracks of the four research aircraft campaigns discussed in this paper. These are OMO (Oxidation Mechanism Observations), ATom (Atmospheric Tomography Mission), CAFE Africa (Chemistry of the Atmosphere Field Experiment in Africa) and CAFE Brazil. The ATom campaign was divided into measurements over the Atlantic and the Pacific Ocean. Detailed information on the individual campaigns and the respective measurements are provided in the following subsections. We filtered all data for the tropical latitudes between 30°S and 30°N and for the troposphere with a threshold of 100 ppbv for O<sub>3</sub>. We use a 1-min average of the measurements, brought to the NO timestamp, for this analysis.

### 2.2.1. OMO 2015

The aircraft campaign OMO (Oxidation Mechanism Observations) took place in July and August 2015 over the Indian Ocean and the Middle East using the HALO (High Altitude Long range) research aircraft. The campaign comprised 17 research flights (some on the same day) with campaign bases in Paphos in Cyprus (34.72°N, 32.49°E) and Gan in the Maldives (0.69°S, 73.16°E). More details can be found in Lelieveld et al. (2018) and Tomsche et al. (2019). Nitric oxide was measured via chemiluminescence with the two-channel AENEAS (Atmospheric nitrogen oxides measuring system) instrument with a detection limit of 7 pptv and a measurement uncertainty of 8% (for 0.5 ppbv) (Stratmann et al., 2016; Ziereis et al., 2000). HO<sub>2</sub> was measured via laser-induced fluorescence with the HORUS (Hydroxyl Radical Measurement Unit based on fluorescence Spectroscopy) and the AirLIF instruments (Künstler, 2020; Marno et al., 2020; Novelli et al., 2014). The HORUS instrument has a detection limit of 1.2 pptv for HO<sub>2</sub> at the surface and 0.23 pptv above 14 km. The accuracy is typically between 20% and 40%. The detection limit and uncertainty for the Air-LIF instrument are also altitude-dependent. The



**Figure 2.** Overview of the flight tracks (filtered by tropical latitudes between 30°S and 30°N) for the four aircraft campaigns OMO (green), ATom, CAFE Africa (red) and CAFE Brazil (blue). The ATom campaign was separated into data over the Atlantic (orange) and the Pacific Ocean (cyan).

detection limit (signal-to-noise ratio = 2, 40 s time resolution) is generally less than 1 pptv and about 0.1 pptv above 5 km. The data accuracy is between 15% and 35%. Neither of the HO<sub>2</sub> measurements was continuous over the entire campaign. The data from the five overlapping flights showed good agreement and we therefore combined the data from the two instruments (research flights 1–6 (21.07.–06.08.2015) from AirLIF and 7–17 (08.08.–27.08.2015) from HORUS) to obtain a full data set. Ozone was measured with the FAIRO (Fast AIRborne Ozone) instrument using a dry chemiluminescence detector, calibrated by a 2-channel UV photometer, with an uncertainty (10 Hz) of 2.5% or 2 ppbv (Obersteiner, 2023; Zahn et al., 2012).

### 2.2.2. ATom 2016–2018

The aircraft campaign ATom (Atmospheric Tomography Mission) consisted of four deployments between 2016 and 2018 in summer 2016, winter 2017, fall 2017 and spring 2018 with the NASA DC-8 aircraft, operated by the NASA Armstrong (Dryden) Flight Research Center. A total of 47 scientific flights were carried out over the almost 2-year period. Each deployment circumnavigated the globe once. More details on the campaign, including all flight tracks, can be found in Thompson et al. (2022) and via the campaign website (NASA, 2022). For this study, we used the data measured in the tropical regions between 30°S and 30°N latitude and additionally separated them into two geographic regions over the Pacific and the Atlantic Ocean (see Figure 2 in cyan and orange, respectively). NO and O<sub>3</sub> were measured via chemiluminescence using an O<sub>3</sub>-induced and a NO-induced technique, respectively. The measurement uncertainties (1 Hz data) were 5% for NO and 2% for O<sub>3</sub>, with a precision of 6 pptv and 15 pptv, respectively (Bourgeois et al., 2021, 2022). HO<sub>2</sub> was measured via laser-induced fluorescence with a 2  $\sigma$  accuracy of 35%. Details can be found in Faloon et al. (2004).

### 2.2.3. CAFE Africa 2018

The Chemistry of the Atmosphere Field Experiment in Africa (CAFE Africa) took place in August and September 2018 from Sal on Cabo Verde (16.75°N, 22.95°W). Fourteen scientific flights were performed with the HALO research aircraft, mostly over the Atlantic Ocean. Details on the campaign and measurements can be found in Tadic et al. (2021). Nitric oxide was measured with the chemiluminescence instrument (CLD 790 SR, ECO Physics, Dürnten, Switzerland) NOAH (Nitrogen Oxides Analyzer for HALO) with a detection limit of 5 pptv (1 min) and an uncertainty of 6%. The instrument is described in detail in Tadic et al. (2020) and Nussbaumer, Parchatka, et al. (2021). Ozone was measured with the FAIRO instrument, as described in Section 2.2.1. HO<sub>2</sub> was measured with the HORUS instrument and has an uncertainty of approximately 50%. Due to the difficulty in determining an experimental calibration factor for the HO<sub>2</sub> data set, a value of 2.5 was estimated based on comparison with the EMAC model and its performance in measuring hydrogen peroxide (H<sub>2</sub>O<sub>2</sub>) (Hamryszczak et al., 2023).

### 2.2.4. CAFE Brazil 2022–2023

The Chemistry of the Atmosphere Field Experiment in Brazil (CAFE Brazil) took place in December 2022 and January 2023 with the HALO research aircraft from Manaus in Brazil (3.03°S, 60.04°W). Twenty scientific flights (including four transfer flights from Oberpfaffenhofen, Germany with a stopover in Sal, Cabo Verde) were carried out over a 2-month period over the pristine rain forest as well as deforested regions and urbanized areas. The scientific goals of the campaign included the investigation of photochemical processes impacted by high VOC/low NO<sub>x</sub> environments, convective events throughout the troposphere and particle formation. The campaign was timed to occur at the seasonal transition which enabled capture of measurements during the dry season in December and the rainy season in January. Nitric oxide was measured with the NOAH instrument with a detection limit of 6 pptv (1 min) and an uncertainty of 5%. O<sub>3</sub> data were obtained with the FAIRO instrument with a data uncertainty of 2.5% or 2 ppbv. Final data for HO<sub>2</sub> measurements are not available at this point and we therefore include modeled data from EMAC simulations, as described in Section 2.3 in our analysis.

## 2.3. Modeling

While this study is based on in situ observations, we include the modeled data for a comparison to identify how well the data sets align. Additionally, we use modeled HO<sub>2</sub> data for CAFE Brazil as final experimental data are not available at this point.

Modeled data for NO, O<sub>3</sub>, HO<sub>2</sub>, temperature, and pressure were obtained with the EMAC model. The ECHAM/MESSy Atmospheric Chemistry (EMAC) model is a numerical chemistry and climate simulation system that includes sub-models describing tropospheric and middle atmosphere processes and their interaction with oceans, land and human influences (Jöckel et al., 2016). It uses the second version of the Modular Earth Submodel System (MESSy2) to link multi-institutional computer codes. The core atmospheric model is the fifth generation European Centre Hamburg general circulation model (Roeckner et al., 2006, ECHAM5). The physics subroutines of the original ECHAM code have been modularized and reimplemented as MESSy submodels and have continuously been further developed. Only the spectral transform core, the flux-form semi-Lagrangian large scale advection scheme, and the nudging routines for Newtonian relaxation are remaining from ECHAM. Here we use different numerical results from different integrations and with different set-up, mostly presented in previous publications. Description of the set-up of the EMAC model for CAFE Africa, OMO, and ATom campaigns can be found in Tadic et al. (2021), Lelieveld et al. (2018), and Nussbaumer et al. (2023), respectively.

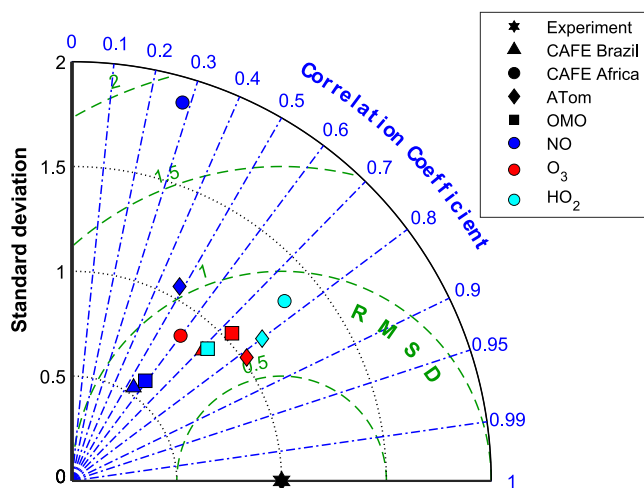
The simulation for the CAFE Brazil measurement campaign was performed at a spectral horizontal resolution of T63, equivalent to approximately 180 × 180 km at the equator, with 90 vertical levels up to an altitude of 0.01 hPa. Weak “nudging” was applied, guiding the simulation toward meteorological reanalysis data (ERA5, Hersbach et al., 2020) from the European Centre for Medium-Range weather forecasts (ECMWF). Global anthropogenic emissions of reactive gases and aerosols at the surface were obtained from the Community Emission Data System (CEDS, McDuffie et al., 2020) and aircraft emission data were taken from the CAMS Global aviation emissions (CAMS-GLOB-AIR; Granier et al., 2019), both for the year 2019.

The simulations for OMO, ATom and CAFE Africa present the same horizontal resolution as the CAFE Brazil simulation, that is, T63. On the other hand, 47 hybrid pressure levels were used to cover the same vertical extension up to 0.01 hPa (instead of 90 levels for CAFE Brazil). In the work of Tadic et al. (2021) and Lelieveld et al. (2018) for CAFE Africa and OMO, respectively, the anthropogenic emissions from EDGARv4.3.2 (Crippa et al., 2018) were used. In Nussbaumer et al. (2023), used for comparison with the ATom observations, the long-term anthropogenic emission data set of CAMS-GLOB-ANTv4.2 (Granier et al., 2019) was adopted. Furthermore, in both the work of Tadic et al. (2021) and Lelieveld et al. (2018), a complex oxidation scheme (MOM) was employed, which has been extensively evaluated in Pozzer et al. (2022). In the work of Nussbaumer et al. (2023) the MIM oxidation scheme was adopted (Pöschl et al., 2000; Taraborrelli et al., 2009). The same algorithms for dry and wet deposition (Kerckweg et al., 2006; Tost et al., 2006) were used in all simulations. Importantly, while the same parameterization was used for lightning NO<sub>x</sub> (Grewe et al., 2001), different scaling factors were employed (Tost et al., 2007). For the ATom and CAFE Africa simulations a total emission of ~6.2 Tg N yr<sup>-1</sup> was used, in accordance with Miyazaki et al. (2014). In contrast, for the OMO simulation a similar amount as for CAFE Brazil was implemented, that is, ~2.6 Tg N yr<sup>-1</sup>, which demonstrates the best agreement with regional observations. These values fall within the estimate of 2–8 Tg N yr<sup>-1</sup> provided by Schumann and Huntrieser (2007).

### 3. Results

#### 3.1. Model Performance

Figure 3 shows a normalized Taylor diagram presenting the model performance for each campaign and trace gas investigated in this analysis (Taylor, 2001). The experimental data is represented by the black hexagram, with a normalized standard deviation of 1, a correlation coefficient of 1 and root-mean-square difference of 0. The closer the colored data points, representing the model data sets, are located to the experimental reference value, the better the model performance. For most of the modeled data sets, standard deviations are similar to those from their experimental counterparts. Deviations are observed for NO (blue): CAFE Brazil (triangles) and OMO data sets (squares) have lower standard deviations by a factor of 2 and the CAFE Africa data set (circles) has a larger standard deviation (almost twice as large). The latter additionally shows only an intermediate correlation coefficient of around 0.3. All other modeled data sets show a good correlation with the experiment with a correlation coefficient of 0.5 or larger. The ATom data set (diamonds) for O<sub>3</sub> even reaches values of >0.8. The O<sub>3</sub> (red) and HO<sub>2</sub> data sets (cyan) for the different campaigns show a similar model performance, whereas differences could be seen between the quality of the different NO data sets. This could be due to the difficulty in accurately representing lightning in the model. A further comparison between modeled and measured data can be found in Figures S1–S5 in Supporting Information S1, where we show the vertical profiles of each trace gas. Tables S1–S5 in



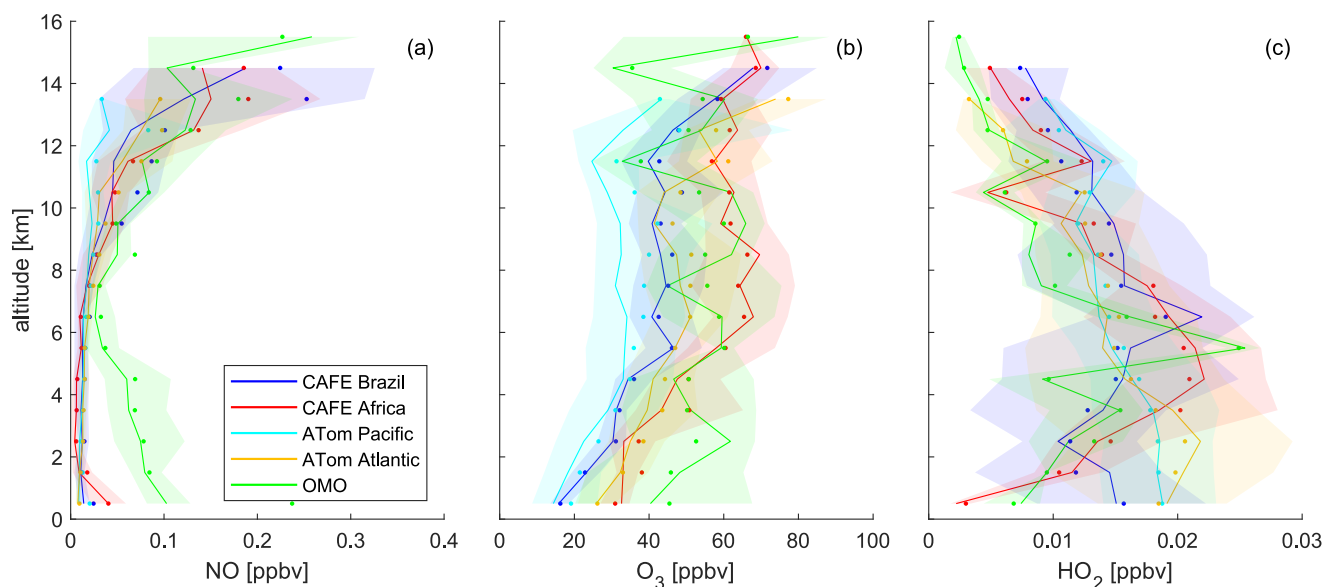
**Figure 3.** Overview of the model performance, presented in a Taylor diagram (Taylor, 2001). The normalized standard deviation is indicated by the black dotted lines, the correlation coefficient is presented by the blue lines and the root-mean-square difference is shown by the green dotted lines. The black hexagram represents the experimental data. Triangles represent modeled data for the CAFE Brazil campaign, circles the CAFE Africa campaign, diamonds the ATom campaign and squares show modeled data for the OMO campaign. Blue colors represent NO, red shows O<sub>3</sub>, and HO<sub>2</sub> data is cyan. The closer the modeled data points are located to the experimental comparison, the better the model performance.

Supporting Information S1 show an overview of the number of data points per altitude bin used to create the vertical profiles. The model may have difficulties representing the intermittent nature of convection and lightning, illustrated by the larger spread in the upper troposphere (UT). HO<sub>2</sub> modeled and experimental vertical profiles align well for OMO, CAFE Africa, and ATom and the Taylor diagram also shows a good model performance, which verifies the use of the modeled HO<sub>2</sub> data set for CAFE Brazil.

### 3.2. Vertical Distribution

Figure 4 presents the vertical profiles of (a) NO, (b) O<sub>3</sub>, and (c) HO<sub>2</sub> measured during the investigated campaigns. During CAFE Brazil, CAFE Africa and ATom over the Pacific and the Atlantic Ocean, NO was low in the lower and middle troposphere with median values below 20 pptv up to 8 km altitude. The values during the OMO campaign were much larger up to 5–6 km; however, only around 5% of all data points were measured at these low altitudes and they were exclusively located in proximity to airports. Therefore, it can be assumed that the large NO mixing ratios represent localized airport emissions. At high altitudes, the profiles show elevated mixing ratios. Above 10 km, NO median values were overall highest during CAFE Africa with 117 pptv, followed by OMO with 108 pptv and CAFE Brazil with 60 pptv. These campaigns were also characterized by large maximum values for NO, sometimes above 1 or 2 ppbv, which indicates strong lightning activity. Median and peak values were generally lower during the ATom campaign with mixing ratios of 51 pptv and 0.43 ppbv, respectively, over the Atlantic and only 20 pptv and 0.48 ppbv, respectively, over the Pacific Ocean. These

observations underline the impact of lightning at these altitudes and latitudes. We have determined a filter for lightning activity which defines data points above 2 km with NO mixing ratios above 100 pptv as impacted by lightning. This includes both fresh and aged lightning emissions. We have tested the performance of this filter via two different methods. First, we investigated NO mixing ratios simulated by the EMAC model as a daily climatology between 2000 and 2020 across all tropical latitudes and altitudes. We filtered for data points between 800 and 200 hPa and with values above 0.1 ppbv. To identify data points above the threshold which did not arise from lightning, we extracted the corresponding data points in a modeled data set excluding lightning emissions.



**Figure 4.** Vertical profiles of (a) NO, (b) O<sub>3</sub>, and (c) HO<sub>2</sub> for tropical latitudes for the investigated aircraft campaigns. Lines and shades represent the median values and the 25th/75th percentiles, respectively. Dots show the mean values in the center of each 1 km altitude bin.

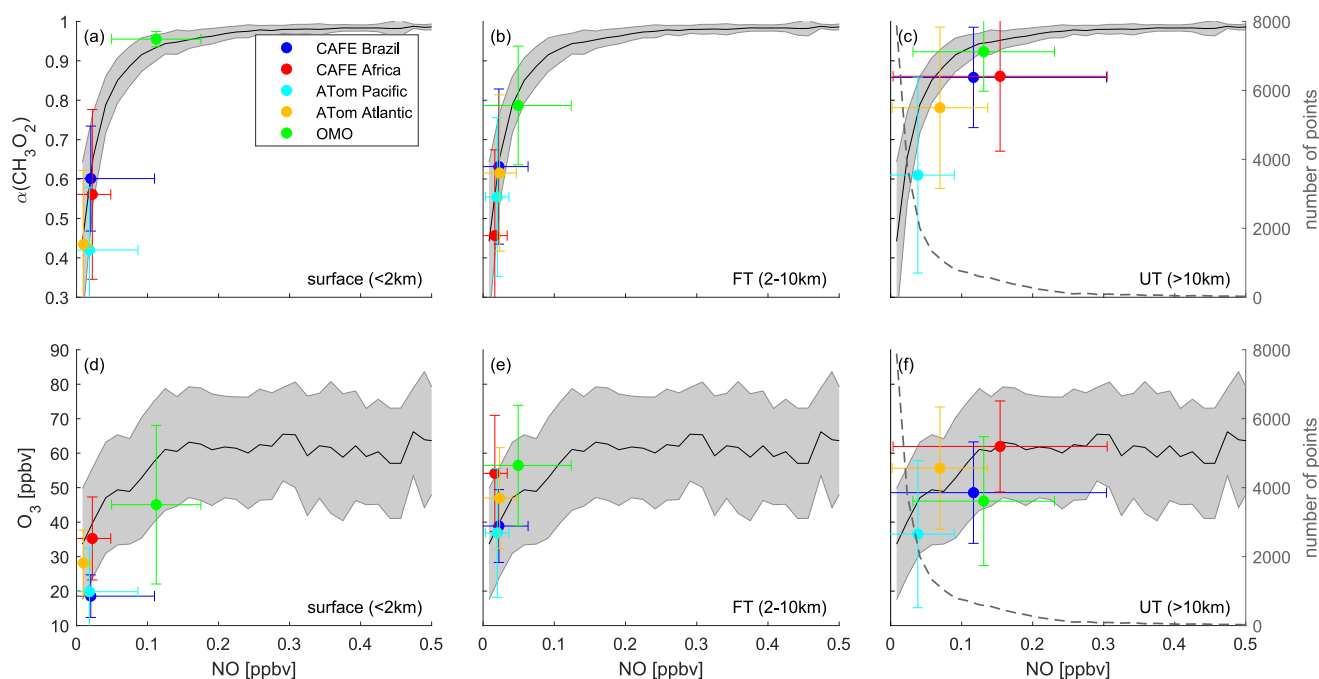


Less than 2% of the remaining data points were larger than 0.1 ppbv. Second, we tested the impact of convective updraft from pollution events, such as wildfires or shipping emissions. For this, we identified data points for which CO was 1.5 or 2  $\sigma$  larger than the average at the respective altitude (bins of 1 km). We compared the share of data points identified as lightning by the filter, including and excluding enhanced CO, and did not find significant differences (deviation <5%). These tests confirm the suitability of the chosen filter. For OMO, this identifies approximately 50% of the data points as being impacted by lightning, followed by CAFE Africa with around 40% and CAFE Brazil with approximately 20%. For ATom, only few data points were impacted by lightning with below 10% over the Atlantic Ocean and less than 5% over the Pacific Ocean, the latter explaining the almost unchanging (with altitude) cyan vertical profile.

These observations demonstrate two important features impacting lightning, which are the time of year and the distance from tropical landmasses. The maximum of deep convection, which is associated with lightning activity and large NO emissions, changes its location throughout the year due to seasonal, meridional changes in convective activity. While over the year as a whole, this maximum is located close to the equator ( $\pm 5^\circ$ ), in January, it is mostly found in the Southern Hemisphere and in July in the Northern Hemisphere (compare Figure 12 in Yan (2005)). The region of maximum deep convection is also referred to as the ITCZ (Inter Tropical Convergence Zone). CAFE Africa and OMO were carried out in August/September mostly coinciding with the location of the ITCZ, explaining high lightning intensity. CAFE Brazil took place in December and January and the flight track latitudes tended to be slightly northward, but still close to the location of the ITCZ at that time of the year, which could be a potential explanation for fewer data points with identified lightning impact. The impact of the time of year can be neglected for the ATom campaign as the vertical profiles present medians and averages across all four deployments. Lightning was lowest over the remote Pacific Ocean during ATom, in line with our understanding of lightning formation, which is thought to require solid particles for the formation of light ice particles. In fact, solid particles, such as dust or sand, are usually more abundant over or in proximity to land masses, which makes lightning strongest over the (tropical) continents (Christian et al., 2003; Nussbaumer, Tadic, et al., 2021; Verma et al., 2021). Pan et al. (2022) presented that sea spray particles could even inhibit lightning activity over oceans. Likewise, low lightning activity was observed over the Atlantic Ocean during ATom. The NO observations for CAFE Africa were much larger in comparison to the ATom Atlantic data in the upper troposphere, although the two data sets are derived from neighboring geographical areas. The location of the ITCZ throughout the year cannot explain the difference, as the median NO mixing ratios measured during the ATom deployment in August were similar to the one in February. However, the ATom Atlantic data set shrinks when filtering the tropical latitudes for different times of the year, whereas CAFE Africa ran many flights in the same region and therefore provides an improved representation of the region. Additional differences may arise from meteorological conditions or differences in wildfire activity between years (ATom Atlantic in August 2016 and CAFE Africa in August 2018).

Figure 4b presents the vertical profiles of O<sub>3</sub>. Generally, O<sub>3</sub> increased with altitude and increasing proximity to the stratosphere, where O<sub>3</sub> is abundant. The lowest mixing ratios were observed during ATom over the Pacific Ocean with median values below 17 ppbv at the surface and 28 ppbv above 10 km. This correlates well with low NO mixing ratios throughout the tropospheric column, which when oxidized to NO<sub>2</sub> is the photochemical source of tropospheric O<sub>3</sub>. The low mixing ratio between 11 and 12 km altitude could indicate convective updraft from the O<sub>3</sub>-poor marine boundary layer. CAFE Brazil O<sub>3</sub> mixing ratios were similar to those observed during ATom Pacific up to 5 km altitude. Above this altitude, O<sub>3</sub> median values during CAFE Brazil were approximately 10–14 ppbv higher. The vertical profile also shows the typical S-shape observed for convective updraft to the upper troposphere. The ATom Atlantic O<sub>3</sub> vertical profile shows a similar shape to the one observed during CAFE Brazil with median mixing ratios of 26 ppbv at the surface and 52 ppbv above 10 km. The vertical O<sub>3</sub> profile for OMO does not show a particular trend with altitude, but a quite strong fluctuation with median values between 30 and 80 ppbv is evident. O<sub>3</sub> mixing ratios during CAFE Africa were around 30 ppbv (median) at the surface and increased strongly up to 60–70 ppbv at 7 km, above which they remained mostly unaffected by altitude. The large difference of around 20 ppbv between O<sub>3</sub> mixing ratios for CAFE Africa and ATom Atlantic in the free troposphere could have likely arisen from the time of year as the profiles align well when only considering August data from the ATom campaign. This could be due to wildfire emissions in the Southern Hemisphere at that time of year.

Figure 4c presents the vertical profiles of HO<sub>2</sub>. Mixing ratios were mostly low and comparable to upper tropospheric values at the surface and showed a maximum in the free troposphere between 3 and 7 km altitude. Quite



**Figure 5.** Overview of determination of  $O_3$  sensitivity via (a)–(c)  $\alpha(\text{CH}_3\text{O}_2)$  and (d)–(f)  $O_3$  versus NO mixing ratios separated into the surface below 2 km (a and d), the free troposphere between 2 and 10 km (b and e) and the upper troposphere above 10 km (c and f). Black lines represent the tropical background as an average of all available data points binned to NO, with  $1\sigma$  standard deviations shown as gray areas. The colored data points and error bars present the campaign averages and  $1\sigma$  standard deviations, respectively. CAFE Brazil averages are shown in blue, CAFE Africa in red, ATom Pacific in cyan, ATom Atlantic in orange and OMO in green. The gray dotted line in panels (c) and (f) shows the number of data points in each NO bin.

large differences between the campaigns can be observed at the surface with median values ranging from around 2 pptv for CAFE Africa and approximately 20 pptv for ATom. However, the uncertainties of the  $\text{HO}_2$  measurements were usually highest at low altitudes and the profiles mostly show large and overlapping error shades (representing the 25th and 75th percentiles). In the upper troposphere,  $\text{HO}_2$  measured during OMO and ATom Atlantic was lowest with a median of 4 pptv above 12 km, followed by CAFE Africa with 7 pptv and CAFE Brazil and ATom Pacific with 10–11 pptv.

### 3.3. $O_3$ Sensitivity

As described above,  $\alpha(\text{CH}_3\text{O}_2)$  can be used to determine  $O_3$  sensitivity to its precursors.  $\alpha(\text{CH}_3\text{O}_2)$  is plotted in Figure 5a–5c for all campaigns. The black line shows the average  $\alpha(\text{CH}_3\text{O}_2)$  binned to NO mixing ratios for all available data points and therefore presents the tropical “background.” The individual curves for each campaign do not show significant differences. As expected,  $\alpha(\text{CH}_3\text{O}_2)$  increases strongly with NO for low ambient NO mixing ratios, which demonstrates  $\text{NO}_x$ -sensitive  $O_3$  chemistry. For an increase in NO from 10 to 100 pptv,  $\alpha(\text{CH}_3\text{O}_2)$  increases by almost 0.5. For higher NO,  $\alpha(\text{CH}_3\text{O}_2)$  becomes unresponsive to changes in NO, which is characteristic of VOC-sensitive  $O_3$  chemistry. For an NO increase from 100 to 500 pptv,  $\alpha(\text{CH}_3\text{O}_2)$  shows an increase of less than 0.1. Panel (c) additionally shows the number of data points in each NO bin by the gray dashed line. The vast majority of the data points is characterized by NO mixing ratios below 0.1 ppbv. The number decreases to a few dozen data points for the high-NO bins. The colored data points represent the campaign averages and the three panels of each row show different altitudes. Figure 5 (a) presents the averages below 2 km altitude. CAFE Brazil, CAFE Africa, ATom Pacific and ATom Atlantic showed a clear  $\text{NO}_x$ -sensitive chemistry at the surface, as the averages are located in the rising part of the background curve of  $\alpha(\text{CH}_3\text{O}_2)$  versus NO. Average values for  $\alpha(\text{CH}_3\text{O}_2)$  were around 0.4 for ATom and close to 0.6 for CAFE Africa and CAFE Brazil, which means that 60% and 40%, respectively, of the available peroxy radicals reacted with  $\text{HO}_2$  and terminated the  $O_3$ -forming  $\text{HO}_x$  cycle. This is expected given low NO mixing ratios in the remote tropical regions or over tropical waters. The OMO data set showed VOC-sensitive  $O_3$  chemistry at the surface with  $\alpha(\text{CH}_3\text{O}_2) = 0.96$ , indicating that almost all peroxy radicals reacted with NO instead of  $\text{HO}_2$ . However, as mentioned above, the very

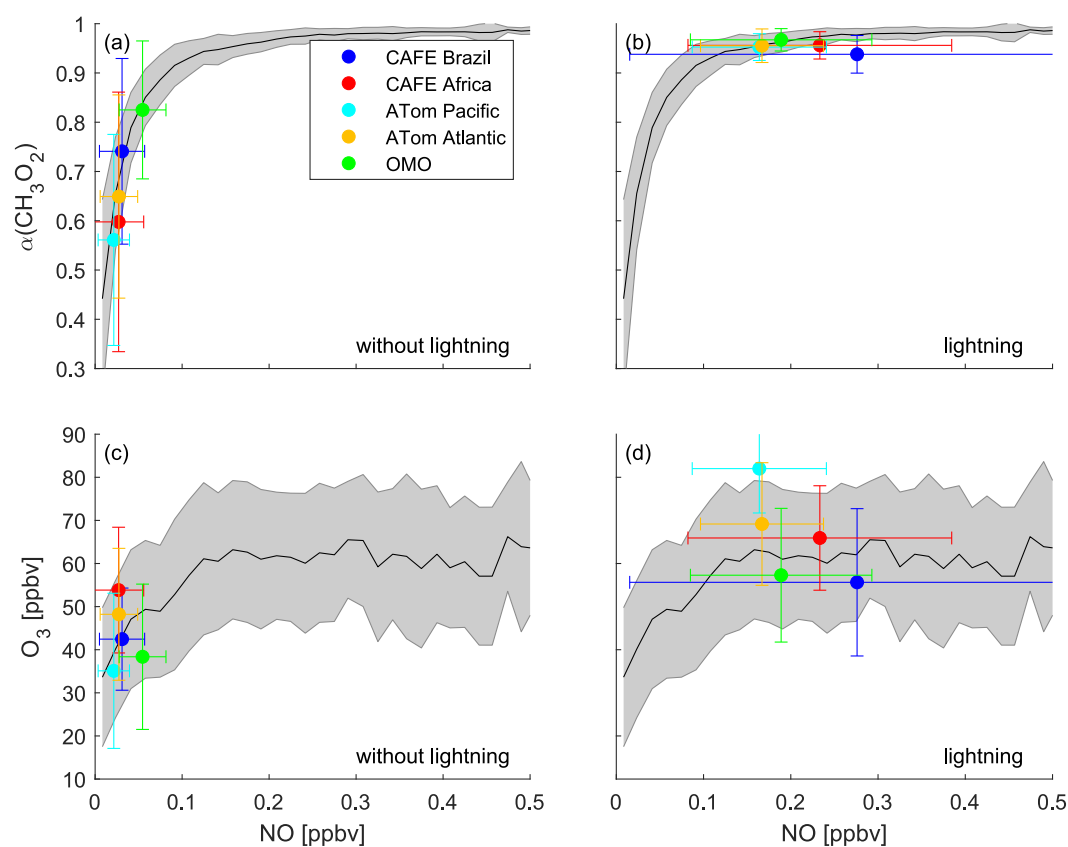
limited number of data points available at low altitude for the OMO campaign were all captured in proximity to airports and therefore do not represent surface conditions in the Middle East or over the Indian Ocean. Figure 5b shows the results for the free troposphere between 2 and 10 km altitude. All campaigns showed a clear  $\text{NO}_x$ -sensitive  $\text{O}_3$  chemistry, which again is expected in the absence of NO sources at these altitudes and aligns with the observations from the vertical profiles in Figure 4. In Figure 5c, upper tropospheric data (above 10 km) are presented. The upper troposphere over the remote Pacific Ocean was clearly  $\text{NO}_x$ -sensitive. The remaining areas were located in a transition regime with average values for  $\alpha(\text{CH}_3\text{O}_2)$  of between 0.78 and 0.92 and for NO of between 0.07 and 0.15 ppbv, whereby ATom Atlantic tended toward  $\text{NO}_x$  sensitivity and the remaining campaigns toward VOC-sensitive  $\text{O}_3$  chemistry. The data points additionally show a large  $1\sigma$  standard deviation in the order of 100% for NO. This underlines the large variability of NO mixing ratios in the upper troposphere caused by clean NO-free air transported from the boundary layer via convective processes and strong, local NO emissions from lightning. We identified <5% and <10% of data points as being impacted by lightning for ATom Pacific and ATom Atlantic, respectively, demonstrating  $\text{NO}_x$ -sensitive chemistry. For the remaining campaigns, lightning impacted a much higher share of data points (~20% for CAFE Brazil, ~40% for CAFE Africa and ~50% for OMO), resulting in higher values for  $\alpha(\text{CH}_3\text{O}_2)$ .

These observations are confirmed when looking at  $\text{O}_3$  versus NO mixing ratios as displayed in the lower panels (d)–(f) of Figure 5. The black line and gray error shading represent background  $\text{O}_3$  binned to NO, including all available data points. For  $\text{NO}_x$ -sensitive chemistry approximately up to 0.1–0.15 ppbv NO,  $\text{O}_3$  increases from 30 to 60 ppbv with increasing NO. Our hypothesis is that in this rising part both peroxy self-reaction and NO to  $\text{NO}_2$  oxidation via peroxy radicals play a significant role, the latter path leading to  $\text{O}_3$  formation in the presence of sunlight and oxygen. With increasing amounts of NO,  $\text{O}_3$  levels rise. In turn, when NO is present in excess over peroxy radicals,  $\text{O}_3$  levels reach a maximum, as its formation is limited by the availability of peroxy radicals. At the surface, as shown in Figure 5d,  $\text{O}_3$  average values for CAFE Brazil, CAFE Africa, ATom Atlantic and ATom Pacific were low, ranging from 20 to 35 ppbv.  $\text{O}_3$  for OMO was higher which correlated with higher NO captured from airport emissions. Slightly higher  $\text{O}_3$  levels between 35 and 55 ppbv were observed for the free troposphere, which can be seen in Figure 5e. These elevated values compared to the surface cannot be explained by photochemical formation in the NO-poor free troposphere, but are likely rather an outcome of transport processes. Upper tropospheric values for  $\text{O}_3$  versus NO are presented in Figure 5f and show similar features compared to  $\alpha(\text{CH}_3\text{O}_2)$  in panel (c). Low average  $\text{O}_3$  (37 ppbv) and NO (0.04 ppbv) indicate  $\text{NO}_x$ -sensitive chemistry in the upper troposphere over the remote Pacific Ocean during the ATom campaign. The remaining data points were located mostly in the transition area. Maximum average values of  $\text{O}_3$  of >60 ppbv were observed for CAFE Africa, going hand-in-hand with high shares of lightning-impacted data. In contrast,  $\text{O}_3$  average values for ATom Atlantic (56 ppbv) were much higher than those observed for OMO (46 ppbv), even though less than 10% of the data points were impacted by lightning during ATom versus 50% during OMO. While the correlation of  $\text{O}_3$  with NO can provide valuable hints for sensitivity investigations, it cannot be solely captured by photochemistry. Instead,  $\text{O}_3$  could also be impacted by transport from the stratosphere or regions with strong tropospheric ozone buildup, for example, biomass burning events, and has a longer upper tropospheric lifetime than NO. The  $\text{O}_3$ -NO correlation should therefore be used in combination with a reliable metric such as  $\alpha(\text{CH}_3\text{O}_2)$ .

### 3.4. Impact of Lightning

We have investigated the role of lightning in  $\text{O}_3$  sensitivity by applying a filter for lightning impact. We categorize data points above 2 km altitude and with NO mixing ratios higher than 0.1 ppbv as impacted by lightning. If the observed NO value is lower, we assume that the data point was not directly impacted by lightning. We expect the contribution of aircraft to the overall  $\text{NO}_x$  emissions in the tropical troposphere to be insignificant (Grewe, 2007; Nussbaumer et al., 2023). Figure 6 presents the  $\text{O}_3$  sensitivity analysis based on  $\alpha(\text{CH}_3\text{O}_2)$  and  $\text{O}_3$  versus NO, following the similar scheme as in Figure 5, separated into data points impacted and not impacted by lightning. The share of data points in each average value depends on the campaign, for example, for ATom Pacific more than 95% fall into the category without lightning, whereas it is 50% for OMO. The background curves are the same as those presented in Figure 5.

Figure 6a shows  $\alpha(\text{CH}_3\text{O}_2)$  versus NO for data points without lightning impact. All five campaign averages were located in the rising part of the background curve with values for  $\alpha(\text{CH}_3\text{O}_2)$  between 0.56 and 0.82, indicating distinct  $\text{NO}_x$ -sensitive  $\text{O}_3$  chemistry. In comparison, Figure 6b presents data points with lightning impact. In all cases, independent of the latitude,  $\alpha(\text{CH}_3\text{O}_2)$  was high and close to 1. This shows that available peroxy radicals



**Figure 6.** Overview of determination of  $O_3$  sensitivity via (a)–(b)  $\alpha(\text{CH}_3\text{O}_2)$  and (c)–(d)  $O_3$  versus NO mixing ratios separated into data with (b and d) and without impact from lightning (a and c).

dominantly reacted with NO resulting in the formation of  $O_3$ , indicating VOC-sensitive chemistry. The  $1\sigma$  standard deviations (shown by the error bars) are quite large because lightning induces highly variable amounts of NO and additionally, we do not distinguish between fresh and aged lightning in this view. For CAFE Brazil, for example, we observed peak values of more than 2 ppbv NO (factor 4 compared to the shown scale).

Figure 6c shows  $O_3$  versus NO for data points not impacted by lightning.  $O_3$  average values ranged between 35 and 55 ppbv. In comparison, the average values impacted by lightning were located at much higher  $O_3$  mixing ratios (between 55 and 80 ppbv) and in the part of the background where  $O_3$  becomes unresponsive to NO, as shown in panel (d). These results support the findings from  $\alpha(\text{CH}_3\text{O}_2)$  and show that lightning plays an important role in the sensitivity of  $O_3$  formation toward its precursors.

#### 4. Conclusion and Outlook

In this study, we presented in situ measurements of NO,  $O_3$  and  $\text{HO}_2$  from four different research aircraft campaigns in the tropical troposphere. These are the OMO campaign in 2015 over the Middle East and the Indian Ocean, the CAFE Africa campaign in 2018 over the Atlantic Ocean, the ATom campaign between 2016 and 2018 around the American continent and the CAFE Brazil campaign in 2022/23 over Brazil. We separated the ATom campaign into a part over the remote Pacific Ocean and a part over the Atlantic Ocean. All data is filtered for the troposphere ( $<100$  ppbv  $O_3$ ) and for tropical latitudes ( $30^\circ\text{S}$ – $30^\circ\text{N}$ ). We compared the in situ measurements with modeled data by the ECHAM5/MESy2 Atmospheric Chemistry (EMAC) model and found good agreement with a correlation coefficient mostly ranging between 0.5 and 0.8 and standard deviations mostly similar to the respective experimental data set. The largest discrepancies were found for the modeled NO for CAFE Africa. Based on these findings, we used the  $\text{HO}_2$  modeled data for CAFE Brazil, as final experimental data were not available. We found low mixing ratios for NO at the surface and in the free troposphere across the remote tropical latitudes, underlining the absence of sources at these altitudes. Mixing ratios in the upper troposphere were

elevated compared to the lower altitudes with highest values over tropical continents (compared to tropical waters), and coincided with the location of maximum deep convection and the ITCZ, where lightning activity peaks. HO<sub>2</sub> was mostly similar in the campaign inter-comparison and large variability made it difficult to identify significant differences. O<sub>3</sub> vertical profiles show signs of deep convective processes, especially for the CAFE Brazil campaign. Mixing ratios were lowest over the remote Pacific Ocean and higher for areas impacted by emissions, for example, biomass burning, such as CAFE Africa.

We investigated O<sub>3</sub> sensitivity using O<sub>3</sub> mixing ratios and the metric  $\alpha(\text{CH}_3\text{O}_2)$  correlated with ambient NO. We found that O<sub>3</sub> chemistry at the surface and the free troposphere was almost exclusively sensitive to NO<sub>x</sub>. The only exception was the OMO campaign, where we observed VOC-sensitive O<sub>3</sub> chemistry at the surface due to the capture of anthropogenic pollution from airports. For the upper troposphere, we found NO<sub>x</sub>-sensitive O<sub>3</sub> chemistry over the remote Pacific Ocean during ATom and a transition regime for the other campaigns, with the value for  $\alpha(\text{CH}_3\text{O}_2)$  increasing with the amount of lightning observed. Separating data points with and without lightning impact showed that lightning is the most important factor controlling O<sub>3</sub> sensitivity in the tropical troposphere. In the absence of lightning, chemistry was NO<sub>x</sub>-sensitive, while it was strongly VOC-sensitive in the presence of lightning, independent of the exact location in the tropical region.

These results are in line with our previous findings in the upper tropical troposphere, which were based entirely on modeling simulations (Nussbaumer et al., 2023). This underlines effectively that  $\alpha(\text{CH}_3\text{O}_2)$  is a powerful metric for identifying O<sub>3</sub> sensitivity and it is applicable both to modeled data and in situ observations. It also shows that NO<sub>x</sub> is the predominant factor determining O<sub>3</sub> sensitivity and in the tropics its major source is lightning, which in turn depends on the time of year and the distance to tropical landmasses. Photochemical O<sub>3</sub> formation is capped by the availability of peroxy radicals in areas impacted by lightning. From this, we conclude that potential increases in lightning in these regions will likely not impact the amount of O<sub>3</sub>, given that levels of peroxy radicals remain unchanged. In turn, increases in lightning in regions that are currently not or only mildly impacted by lightning might lead to increases of O<sub>3</sub> levels up to a factor of 2, which could strongly impact the radiative forcing (especially at high altitudes). The remote tropical lower troposphere currently has only a small number of NO sources. This could change in the future if biomass burning events would become more frequent with increasing temperature and decreasing precipitation and if countries in the Global South increase NO<sub>x</sub> emissions associated with the expansion of their economies. Combined with NO<sub>x</sub>-sensitive O<sub>3</sub> chemistry, this would lead to strong increases of O<sub>3</sub> levels, which could locally harm plants and human health or, given the lifetime of O<sub>3</sub> of a few weeks, be transported to areas where it has adverse effects.

Looking into the future, further research should investigate the changing role of NO<sub>x</sub> in tropospheric O<sub>3</sub> chemistry. While we can say that NO<sub>x</sub> is the most important driver of O<sub>3</sub> sensitivity, future changes and North-South re-locations in NO<sub>x</sub> emissions, such as expected changes in emissions from anthropogenic combustion processes or increases in biomass burning, will profoundly influence tropospheric photochemistry, and in turn air quality and climate change.

## Data Availability Statement

The data set for the OMO campaign can be obtained from the HALO database (last access: 23.10.2023) (Deutsches Zentrum für Luft- und Raumfahrt (DLR), 2021). The ATom data set is available at Wofsy et al. (2021) (last access: 15.09.2023). The data sets for CAFE Africa and CAFE Brazil can be accessed at Nussbaumer et al. (2024).

## References

- Ainsworth, E. A., Yendrek, C. R., Sitch, S., Collins, W. J., & Emberson, L. D. (2012). The effects of tropospheric ozone on net primary productivity and implications for climate change. *Annual Review of Plant Biology*, 63(1), 637–661. <https://doi.org/10.1146/annurev-arplant-042110-103829>
- Akimoto, H., & Tanimoto, H. (2022). Rethinking of the adverse effects of NO<sub>x</sub>-control on the reduction of methane and tropospheric ozone—challenges toward a denitrified society. *Atmospheric Environment*, 277, 119033. <https://doi.org/10.1016/j.atmosenv.2022.119033>
- Archibald, A. T., Neu, J. L., Elshorbany, Y. F., Cooper, O. R., Young, P. J., Akiyoshi, H., et al. (2020). Tropospheric ozone assessment report: A critical review of changes in the tropospheric ozone burden and budget from 1850 to 2100. *Elementa: Science of the Anthropocene*, 8(1), 034. <https://doi.org/10.1525/elementa.2020.034>
- Bourgeois, I., Peischl, J., Neuman, J. A., Brown, S. S., Allen, H. M., Campuzano-Jost, P., et al. (2022). Comparison of airborne measurements of NO, NO<sub>2</sub>, HONO, NO<sub>y</sub>, and CO during FIREX-AQ. *Atmospheric Measurement Techniques*, 15(16), 4901–4930. <https://doi.org/10.5194/amt-15-4901-2022>

## Acknowledgments

We thank Uwe Parchatka for his support with the NO<sub>x</sub> measurements. We acknowledge the German Aerospace Center (DLR) for the collaboration during CAFE Africa and CAFE Brazil. Open Access funding enabled and organized by Projekt DEAL.

- Bourgeois, I., Peischl, J., Neuman, J. A., Brown, S. S., Thompson, C. R., Aikin, K. C., et al. (2021). Large contribution of biomass burning emissions to ozone throughout the global remote troposphere. *Proceedings of the National Academy of Sciences*, 118(52), e2109628118. <https://doi.org/10.1073/pnas.2109628118>
- Brasseur, G. P., Müller, J.-F., & Granier, C. (1996). Atmospheric impact of NO<sub>x</sub> emissions by subsonic aircraft: A three-dimensional model study. *Journal of Geophysical Research*, 101(D1), 1423–1428. <https://doi.org/10.1029/95JD02363>
- Bray, C. D., Batty, W. H., Aneja, V. P., & Schlesinger, W. H. (2021). Global emissions of NH<sub>3</sub>, NO<sub>x</sub>, and N<sub>2</sub>O from biomass burning and the impact of climate change. *Journal of the Air & Waste Management Association*, 71(1), 102–114. <https://doi.org/10.1080/10962247.2020.1842822>
- Christian, H. J., Blakeslee, R. J., Boccippio, D. J., Boeck, W. L., Buechler, D. E., Driscoll, K. T., et al. (2003). Global frequency and distribution of lightning as observed from space by the optical transient detector. *Journal of Geophysical Research*, 108(D1), ACL4-1–ACL4-15. <https://doi.org/10.1029/2002JD002347>
- Cooper, O. R., Parrish, D., Ziemke, J., Balashov, N., Cupeiro, M., Galbally, I., et al. (2014). Global distribution and trends of tropospheric ozone: An observation-based review. *Elementa: Science of the Anthropocene*, 2. <https://doi.org/10.12952/journal.elementa.000029>
- Crippa, M., Guizzardi, D., Muntean, M., Schaaf, E., Dentener, F., van Aardenne, J. A., et al. (2018). Gridded emissions of air pollutants for the period 1970–2012 within Edgar v4. 3.2. *Earth System Science Data*, 10(4), 1987–2013. <https://doi.org/10.5194/essd-10-1987-2018>
- Crutzen, P. J. (1988). *Tropospheric ozone: An overview*. Springer. [https://doi.org/10.1007/978-94-009-2913-5\\_1](https://doi.org/10.1007/978-94-009-2913-5_1)
- Deutsches Zentrum für Luft- und Raumfahrt (DLR). (2021). Mission:OMO [Dataset]. DLR. Retrieved from <https://halo-db.pa.op.dlr.de/mision/0>
- Duncan, B. N., Yoshida, Y., Olson, J. R., Sillman, S., Martin, R. V., Lamsal, L., et al. (2010). Application of OMI observations to a space-based indicator of NO<sub>x</sub> and VOC controls on surface ozone formation. *Atmospheric Environment*, 44(18), 2213–2223. <https://doi.org/10.1016/j.atmosenv.2010.03.010>
- Faloona, I. C., Tan, D., Leshner, R. L., Hazen, N. L., Frame, C. L., Simpkins, J. B., et al. (2004). A laser-induced fluorescence instrument for detecting tropospheric OH and HO<sub>2</sub>: Characteristics and calibration. *Journal of Atmospheric Chemistry*, 47(2), 139–167. <https://doi.org/10.1023/B:JOCH.0000021036.53185.0e>
- Fujita, E. M., Stockwell, W. R., Campbell, D. E., Keislar, R. E., & Lawson, D. R. (2003). Evolution of the magnitude and spatial extent of the weekend ozone effect in California's south coast air basin, 1981–2000. *Journal of the Air & Waste Management Association*, 53(7), 802–815. <https://doi.org/10.1080/10473289.2003.10466225>
- Gaudel, A., Bourgeois, I., Li, M., Chang, K.-L., Ziemke, J., Sauvage, B., et al. (2024). Tropical tropospheric ozone distribution and trends from in situ and satellite data. *EGU sphere*, 2024, 1–51. <https://doi.org/10.5194/egusphere-2023-3095>
- Gough, W. A., & Anderson, V. (2022). Changing air quality and the ozone weekend effect during the COVID-19 pandemic in Toronto, Ontario, Canada. *Climate*, 10(3), 41. <https://doi.org/10.3390/cli10030041>
- Granier, C., Darras, S., Denier van der Gon, H., Doubalova, J., Elguindi, N., Galle, B., et al. (2019). The copernicus atmosphere monitoring service global and regional emissions (April 2019 version). *Copernicus Atmosphere Monitoring Service (CAMS) report*. <https://doi.org/10.24380/d0bn-kx16>
- Grewe, V. (2007). Impact of climate variability on tropospheric ozone. *Science of the total environment*, 374(1), 167–181. <https://doi.org/10.1016/j.scitotenv.2007.01.032>
- Grewe, V., Brunner, D., Dameris, M., Grenfell, J., Hein, R., Shindell, D., & Staehelin, J. (2001). Origin and variability of upper tropospheric nitrogen oxides and ozone at northern mid-latitudes. *Atmospheric Environment*, 35(20), 3421–3433. [https://doi.org/10.1016/S1352-2310\(01\)00134-0](https://doi.org/10.1016/S1352-2310(01)00134-0)
- Hamryszczak, Z., Dienhart, D., Brendel, B., Rohloff, R., Marno, D., Martinez, M., et al. (2023). Measurement report: Hydrogen peroxide in the upper tropical troposphere over the Atlantic Ocean and western Africa during the cafe-Africa aircraft campaign. *Atmospheric Chemistry and Physics*, 23(10), 5929–5943. <https://doi.org/10.5194/acp-23-5929-2023>
- Hersbach, H., Bell, B., Berrisford, P., Hirahara, S., Horányi, A., Muñoz-Sabater, J., et al. (2020). The ERA5 global reanalysis. *Quarterly Journal of the Royal Meteorological Society*, 146(730), 1999–2049. <https://doi.org/10.1002/qj.3803>
- Iglesias-Suarez, F., Kinnison, D. E., Rap, A., Maycock, A. C., Wild, O., & Young, P. J. (2018). Key drivers of ozone change and its radiative forcing over the 21st century. *Atmospheric Chemistry and Physics*, 18(9), 6121–6139. <https://doi.org/10.5194/acp-18-6121-2018>
- IPCC. (2023). Sections. In H. Lee & J. Romero (Eds.), *Climate change 2023: Synthesis report. Contribution of working groups I, II and III to the sixth assessment report of the intergovernmental panel on climate change [core writing team]* (pp. 35–115). <https://doi.org/10.59327/IPCC/AR6-9789291691647>
- IUPAC. (2024). Evaluated kinetic data. Retrieved from <https://iupac.aeris-data.fr/>
- Jaeglé, L., Jacob, D. J., Brune, W., Faloona, I., Tan, D., Kondo, Y., et al. (1999). Ozone production in the upper troposphere and the influence of aircraft during SONEX: Approach of NO<sub>x</sub>-saturated conditions. *Geophysical Research Letters*, 26(20), 3081–3084. <https://doi.org/10.1029/1999GL900451>
- Jaeglé, L., Jacob, D. J., Brune, W., Tan, D., Faloona, I., Weinheimer, A., et al. (1998). Sources of HO<sub>x</sub> and production of ozone in the upper troposphere over the United States. *Geophysical Research Letters*, 25(10), 1709–1712. <https://doi.org/10.1029/98GL00041>
- Jaffe, D. A., Ninneman, M., & Chan, H. C. (2022). NO<sub>x</sub> and O<sub>3</sub> trends at us non-attainment areas for 1995–2020: Influence of COVID-19 reductions and wildland fires on policy-relevant concentrations. *Journal of Geophysical Research: Atmospheres*, 127(11), e2021JD036385. <https://doi.org/10.1029/2021JD036385>
- Jöckel, P., Tost, H., Pozzer, A., Kunze, M., Kirner, O., Brenninkmeijer, C. A., et al. (2016). Earth system chemistry integrated modelling (ESCIIMO) with the modular Earth submodel system (MESSY) version 2.51. *Geoscientific Model Development*, 9(3), 1153–1200. <https://doi.org/10.5194/gmd-9-1153-2016>
- Kerkweg, A., Buchholz, J., Ganzeveld, L., Pozzer, A., Tost, H., & Jöckel, P. (2006). Technical note: An implementation of the dry removal processes dry deposition and sedimentation in the modular earth submodel system (MESSY). *Atmospheric Chemistry and Physics*, 6(12), 4617–4632. <https://doi.org/10.5194/acp-6-4617-2006>
- Künstler, C. (2020). Measurements of atmospheric OH and HO<sub>2</sub> radicals by laser-induced fluorescence on the halo aircraft during the OMO-Asia 2015 campaign. *Doctoral dissertation, Universität zu Köln*. Retrieved from <http://kups.ub.uni-koeln.de/id/eprint/11702>
- Lacis, A. A., Wuebbles, D. J., & Logan, J. A. (1990). Radiative forcing of climate by changes in the vertical distribution of ozone. *Journal of Geophysical Research*, 95(D7), 9971–9981. <https://doi.org/10.1029/JD095iD07p09971>
- Lelieveld, J., Bourtsoukidis, E., Brühl, C., Fischer, H., Fuchs, H., Harder, H., et al. (2018). The south Asian monsoon—Pollution pump and purifier. *Science*, 361(6399), 270–273. <https://doi.org/10.1126/science.aar2501>
- Lelieveld, J., & Dentener, F. J. (2000). What controls tropospheric ozone? *Journal of Geophysical Research*, 105(D3), 3531–3551. <https://doi.org/10.1029/1999JD901011>

- Lelieveld, J., Gromov, S., Pozzer, A., & Taraborrelli, D. (2016). Global tropospheric hydroxyl distribution, budget and reactivity. *Atmospheric Chemistry and Physics*, 16(19), 12477–12493. <https://doi.org/10.5194/acp-16-12477-2016>
- Li, K., Jacob, D. J., Liao, H., Shen, L., Zhang, Q., & Bates, K. H. (2019). Anthropogenic drivers of 2013–2017 trends in summer surface ozone in China. *Proceedings of the National Academy of Sciences of the United States of America*, 116(2), 422–427. <https://doi.org/10.1073/pnas.1812168116>
- Liu, C., & Shi, K. (2021). A review on methodology in O<sub>3</sub>-NO<sub>x</sub>-VOC sensitivity study. *Environmental Pollution*, 291, 118249. <https://doi.org/10.1016/j.envpol.2021.118249>
- Marno, D., Ernest, C., Hens, K., Javed, U., Klimach, T., Martinez, M., et al. (2020). Calibration of an airborne HO<sub>x</sub> instrument using the all pressure altitude-based calibrator for HO<sub>x</sub> experimentation (Apache). *Atmospheric Measurement Techniques*, 13(5), 2711–2731. <https://doi.org/10.5194/amt-13-2711-2020>
- McDonald, B. C., De Gouw, J. A., Gilman, J. B., Jathar, S. H., Akherati, A., Cappa, C. D., et al. (2018). Volatile chemical products emerging as largest petrochemical source of urban organic emissions. *Science*, 359(6377), 760–764. <https://doi.org/10.1126/science.aag0524>
- McDuffie, E. E., Smith, S. J., O'Rourke, P., Tibrewal, K., Venkataraman, C., Marais, E. A., et al. (2020). A global anthropogenic emission inventory of atmospheric pollutants from sector- and fuel-specific sources (1970–2017): An application of the community emissions data system (CEDS). *Earth System Science Data*, 12(4), 3413–3442. <https://doi.org/10.5194/essd-12-3413-2020>
- Miyazaki, K., Eskes, H. J., Sudo, K., & Zhang, C. (2014). Global lightning NO<sub>x</sub> production estimated by an assimilation of multiple satellite data sets. *Atmospheric Chemistry and Physics*, 14(7), 3277–3305. <https://doi.org/10.5194/acp-14-3277-2014>
- NASA. (2022). ATom. Retrieved from <https://espo.nasa.gov/atom>
- Novelli, A., Hens, K., Tatum Ernest, C., Kubistin, D., Regelin, E., Elste, T., et al. (2014). Characterisation of an inlet pre-injector laser-induced fluorescence instrument for the measurement of atmospheric hydroxyl radicals. *Atmospheric Measurement Techniques*, 7(10), 3413–3430. <https://doi.org/10.5194/amt-7-3413-2014>
- Nussbaumer, C. M. (2023). Nitrogen oxides and their involvement in photochemical processes throughout the troposphere (Doctoral dissertation, Universität Mainz). <https://doi.org/10.25358/openscience-9272>
- Nussbaumer, C. M., & Cohen, R. C. (2020). The role of temperature and NO<sub>x</sub> in ozone trends in the Los Angeles basin. *Environmental Science & Technology*, 54(24), 15652–15659. <https://doi.org/10.1021/acs.est.0c04910>
- Nussbaumer, C. M., Crowley, J. N., Schuladen, J., Williams, J., Hafermann, S., Reiffs, A., et al. (2021). Measurement report: Photochemical production and loss rates of formaldehyde and ozone across Europe. *Atmospheric Chemistry and Physics*, 21(24), 18413–18432. <https://doi.org/10.5194/acp-21-18413-2021>
- Nussbaumer, C. M., Fischer, H., Lelieveld, J., & Pozzer, A. (2023). What controls ozone sensitivity in the upper tropical troposphere? *Atmospheric Chemistry and Physics*, 23(19), 12651–12669. <https://doi.org/10.5194/acp-23-12651-2023>
- Nussbaumer, C. M., Kohl, M., Pozzer, A., Tadic, I., Rohloff, R., Marno, D., et al. (2024). Supporting data for: Ozone Formation Sensitivity to Precursors and Lightning in the Tropical Troposphere Based on Airborne Observations [Dataset]. *Zenodo*. <https://doi.org/10.5281/zenodo.12744436>
- Nussbaumer, C. M., Parchatka, U., Tadic, I., Bohn, B., Marno, D., Martinez, M., et al. (2021). Modification of a conventional photolytic converter for improving aircraft measurements of NO<sub>2</sub> via chemiluminescence. *Atmospheric Measurement Techniques*, 14(10), 6759–6776. <https://doi.org/10.5194/amt-14-6759-2021>
- Nussbaumer, C. M., Pozzer, A., Tadic, I., Röder, L., Obersteiner, F., Harder, H., et al. (2022). Tropospheric ozone production and chemical regime analysis during the COVID-19 lockdown over Europe. *Atmospheric Chemistry and Physics*, 22(9), 6151–6165. <https://doi.org/10.5194/acp-22-6151-2022>
- Nussbaumer, C. M., Tadic, I., Dienhart, D., Wang, N., Edtbauer, A., Ernlé, L., et al. (2021). Measurement report: In situ observations of deep convection without lightning during the tropical cyclone Florence 2018. *Atmospheric Chemistry and Physics*, 21(10), 7933–7945. <https://doi.org/10.5194/acp-21-7933-2021>
- Nuvolone, D., Petri, D., & Voller, F. (2018). The effects of ozone on human health. *Environmental Science and Pollution Research*, 25(9), 8074–8088. <https://doi.org/10.1007/s11356-017-9239-3>
- Obersteiner, F. (2023). FairO. <https://doi.org/10.5281/zenodo.11104075>
- Pan, Z., Mao, F., Rosenfeld, D., Zhu, Y., Zang, L., Lu, X., et al. (2022). Coarse sea spray inhibits lightning. *Nature Communications*, 13(1), 4289. <https://doi.org/10.1038/s41467-022-31714-5>
- Pope, R. J., Arnold, S. R., Chipperfield, M. P., Reddington, C. L., Butt, E. W., Kestlake, T. D., et al. (2020). Substantial increases in eastern amazon and cerrado biomass burning-sourced tropospheric ozone. *Geophysical Research Letters*, 47(3), e2019GL084143. <https://doi.org/10.1029/2019GL084143>
- Pöschl, U., von Kuhlmann, R., Poisson, N., & Crutzen, P. J. (2000). Development and intercomparison of condensed isoprene oxidation mechanisms for global atmospheric modeling. *Journal of Atmospheric Chemistry*, 37(1), 29–52. <https://doi.org/10.1023/A:1006391009798>
- Pozzer, A., Reifenberg, S. F., Kumar, V., Franco, B., Kohl, M., Taraborrelli, D., et al. (2022). Simulation of organics in the atmosphere: Evaluation of emacv2. 54 with the Mainz organic mechanism (MOM) coupled to the oracle (v1. 0) submodel. *Geoscientific Model Development*, 15(6), 2673–2710. <https://doi.org/10.5194/gmd-15-2673-2022>
- Pusede, S. E., Steiner, A. L., & Cohen, R. C. (2015). Temperature and recent trends in the chemistry of continental surface ozone. *Chemical reviews*, 115(10), 3898–3918. <https://doi.org/10.1021/cr5006815>
- Roeckner, E., Brokopf, R., Esch, M., Giorgetta, M., Hagemann, S., Kornbluh, L., et al. (2006). Sensitivity of simulated climate to horizontal and vertical resolution in the ECHAM5 atmosphere model. *Journal of Climate*, 19(16), 3771–3791. <https://doi.org/10.1175/jcli3824.1>
- Schroeder, J. R., Crawford, J. H., Fried, A., Walega, J., Weinheimer, A., Wisthaler, A., et al. (2017). New insights into the column CH<sub>2</sub>O/NO<sub>2</sub> ratio as an indicator of near-surface ozone sensitivity. *Journal of Geophysical Research: Atmospheres*, 122(16), 8885–8907. <https://doi.org/10.1002/2017JD026781>
- Schumann, U., & Huntrieser, H. (2007). The global lightning-induced nitrogen oxides source. *Atmospheric Chemistry and Physics*, 7(14), 3823–3907. <https://doi.org/10.5194/acp-7-3823-2007>
- Shah, V., Jacob, D. J., Dang, R., Lamsal, L. N., Strode, S. A., Steenrod, S. D., et al. (2023). Nitrogen oxides in the free troposphere: Implications for tropospheric oxidants and the interpretation of satellite no<sub>2</sub> measurements. *Atmospheric Chemistry and Physics*, 23(2), 1227–1257. <https://doi.org/10.5194/acp-23-1227-2023>
- Sicard, P., Paoletti, E., Agathokleous, E., Araminiené, V., Proietti, C., Coulibaly, F., & De Marco, A. (2020). Ozone weekend effect in cities: Deep insights for urban air pollution control. *Environmental Research*, 191, 110193. <https://doi.org/10.1016/j.envres.2020.110193>
- Sillman, S. (1995). The use of NO<sub>y</sub>, H<sub>2</sub>O<sub>2</sub>, and HNO<sub>3</sub> as indicators for ozone-NO<sub>x</sub>-hydrocarbon sensitivity in urban locations. *Journal of Geophysical Research*, 100(D7), 14175–14188. <https://doi.org/10.1029/94JD02953>

- Sillman, S., & He, D. (2002). Some theoretical results concerning O<sub>3</sub>-NO<sub>x</sub>-VOC chemistry and NO<sub>x</sub>-VOC indicators. *Journal of Geophysical Research*, 107(D22), ACH26-1–ACH26-15. <https://doi.org/10.1029/2001JD001112>
- Skeie, R. B., Myhre, G., Hodnebrog, Ø., Cameron-Smith, P. J., Deushi, M., Hegglin, M. I., et al. (2020). Historical total ozone radiative forcing derived from CMIP6 simulations. *Npj Climate and Atmospheric Science*, 3(1), 32. <https://doi.org/10.1038/s41612-020-00131-0>
- Souri, A. H., Johnson, M. S., Wolfe, G. M., Crawford, J. H., Fried, A., Wisthaler, A., et al. (2023). Characterization of errors in satellite-based HCHO/NO<sub>2</sub> tropospheric column ratios with respect to chemistry, column-to-PBL translation, spatial representation, and retrieval uncertainties. *Atmospheric Chemistry and Physics*, 23(3), 1963–1986. <https://doi.org/10.5194/acp-23-1963-2023>
- Souri, A. H., Nowlan, C. R., Wolfe, G. M., Lamsal, L. N., Miller, C. E. C., Abad, G. G., et al. (2020). Revisiting the effectiveness of HCHO/NO<sub>2</sub> ratios for inferring ozone sensitivity to its precursors using high resolution airborne remote sensing observations in a high ozone episode during the KORUS-AQ campaign. *Atmospheric Environment*, 224, 117341. <https://doi.org/10.1016/j.atmosenv.2020.117341>
- Staehelin, J., Harris, N. R., Appenzeller, C., & Eberhard, J. (2001). Ozone trends: A review. *Reviews of Geophysics*, 39(2), 231–290. <https://doi.org/10.1029/1999RG000059>
- Stratmann, G., Ziereis, H., Stock, P., Brenninkmeijer, C., Zahn, A., Rauthe-Schöch, A., et al. (2016). NO and NO<sub>y</sub> in the upper troposphere: Nine years of Caribic measurements onboard a passenger aircraft. *Atmospheric Environment*, 133, 93–111. <https://doi.org/10.1016/j.atmosenv.2016.02.035>
- Tadic, I., Crowley, J. N., Dienhart, D., Eger, P., Harder, H., Hottmann, B., et al. (2020). Net ozone production and its relationship to nitrogen oxides and volatile organic compounds in the marine boundary layer around the Arabian Peninsula. *Atmospheric Chemistry and Physics*, 20(11), 6769–6787. <https://doi.org/10.5194/acp-20-6769-2020>
- Tadic, I., Nussbaumer, C., Bohn, B., Harder, H., Marno, D., Martinez, M., et al. (2021). Central role of nitric oxide in ozone production in the upper tropical troposphere over the Atlantic Ocean and West Africa. *Atmospheric Chemistry and Physics*, 21(10), 8195–8211. <https://doi.org/10.5194/acp-2021-52>
- Taraborrelli, D., Lawrence, M., Butler, T., Sander, R., & Lelieveld, J. (2009). Mainz isoprene mechanism 2 (MIM2): An isoprene oxidation mechanism for regional and global atmospheric modelling. *Atmospheric Chemistry and Physics*, 9(8), 2751–2777. <https://doi.org/10.5194/acp-9-2751-2009>
- Taylor, K. E. (2001). Summarizing multiple aspects of model performance in a single diagram. *Journal of Geophysical Research*, 106(D7), 7183–7192. <https://doi.org/10.1029/2000JD900719>
- Thompson, C. R., Wofsy, S. C., Prather, M. J., Newman, P. A., Hanisco, T. F., Ryerson, T. B., et al. (2022). The NASA atmospheric tomography (ATOM) mission: Imaging the chemistry of the global atmosphere. *Bulletin of the American Meteorological Society*, 103(3), E761–E790. <https://doi.org/10.1175/BAMS-D-20-0315.1>
- Tomsche, L., Pozzer, A., Ojha, N., Parchatka, U., Lelieveld, J., & Fischer, H. (2019). Upper tropospheric CH<sub>4</sub> and CO affected by the south Asian summer monsoon during the oxidation mechanism observations mission. *Atmospheric Chemistry and Physics*, 19(3), 1915–1939. <https://doi.org/10.5194/acp-19-1915-2019>
- Tonnesen, G. S., & Dennis, R. L. (2000). Analysis of radical propagation efficiency to assess ozone sensitivity to hydrocarbons and NO<sub>x</sub>: 2. Long-lived species as indicators of ozone concentration sensitivity. *Journal of Geophysical Research*, 105(D7), 9227–9241. <https://doi.org/10.1029/1999JD900372>
- Tost, H., Jöckel, P., Kerkweg, A., Sander, R., & Lelieveld, J. (2006). Technical note: A new comprehensive scavenging submodel for global atmospheric chemistry modelling. *Atmospheric Chemistry and Physics*, 6(3), 565–574. <https://doi.org/10.5194/acp-6-565-2006>
- Tost, H., Jöckel, P., & Lelieveld, J. (2007). Lightning and convection parameterisations – Uncertainties in global modelling. *Atmospheric Chemistry and Physics*, 7(17), 4553–4568. <https://doi.org/10.5194/acp-7-4553-2007>
- Verma, S., Yadava, P. K., Lal, D., Mall, R., Kumar, H., & Payra, S. (2021). Role of lightning NO<sub>x</sub> in ozone formation: A review. *Pure and Applied Geophysics*, 178(4), 1425–1443. <https://doi.org/10.1007/s00024-021-02710-5>
- Vermeuel, M. P., Novak, G. A., Alwe, H. D., Hughes, D. D., Kaleel, R., Dickens, A. F., et al. (2019). Sensitivity of ozone production to NO<sub>x</sub> and VOC along the Lake Michigan coastline. *Journal of Geophysical Research: Atmospheres*, 124(20), 10989–11006. <https://doi.org/10.1029/2019JD030842>
- Wennberg, P., Hanisco, T., Jaegle, L., Jacob, D., Hints, E., Lanzendorf, E., et al. (1998). Hydrogen radicals, nitrogen radicals, and the production of O<sub>3</sub> in the upper troposphere. *Science*, 279(5347), 49–53. <https://doi.org/10.1126/science.279.5347.49>
- Wofsy, S., Afshar, S., Allen, H., Apel, E., Asher, E., Barletta, B., et al. (2021). ATom: Merged Atmospheric Chemistry, Trace Gases, and Aerosols, Version 2 [Dataset]. *ORNL Distributed Active Archive Center*. <https://doi.org/10.3334/ORNLDAAC/1925>
- Yan, Y. Y. (2005). Intertropical convergence zone (ITCZ). In *Encyclopedia of world climatology* (pp. 429–432). Springer Netherlands. [https://doi.org/10.1007/1-4020-3266-8\\_110](https://doi.org/10.1007/1-4020-3266-8_110)
- Zahn, A., Weppner, J., Widmann, H., Schlote-Holubek, K., Burger, B., Kühner, T., & Franke, H. (2012). A fast and precise chemiluminescence ozone detector for eddy flux and airborne application. *Atmospheric Measurement Techniques*, 5(2), 363–375. <https://doi.org/10.5194/amt-5-363-2012>
- Zhao, Y., Li, Y., Kumar, A., Ying, Q., Vandenberghe, F., & Kleeman, M. J. (2022). Separately resolving NO<sub>x</sub> and VOC contributions to ozone formation. *Atmospheric Environment*, 285, 119224. <https://doi.org/10.1016/j.atmosenv.2022.119224>
- Ziereis, H., Schlager, H., Schulte, P., Van Velthoven, P., & Slemr, F. (2000). Distributions of NO, NO<sub>x</sub>, and NO<sub>y</sub> in the upper troposphere and lower stratosphere between 28 and 61 N during Polinat 2. *Journal of Geophysical Research*, 105(D3), 3653–3664. <https://doi.org/10.1029/1999JD90087>